Properties and Reactivities of the Hydrido Ligands in Iridium Sulfido Clusters Relevant to Activation and Production of H_2

Hidetake Seino,* Akihiro Saito, Hidenobu Kajitani, and Yasushi Mizobe*

Institute of Industrial Science, The University of Tokyo, Komaba, Meguro-ku, Tokyo 153-8505, Japan

Received December 3, 2007

Sulfido-hydrido clusters whose cores consist of three to six iridium atoms, $[(Cp^*Ir)_3(\mu_3\text{-}S)(\mu_2\text{-}H)_3][BF_4]$ (**2**), $[(Cp^*Ir)_4(\mu_3\text{-}S)_2(\mu_2\text{-}H)_3][BF_4]$ (**3**), $[(Cp^*IrH)_2(Cp^*Ir)(\mu_3\text{-}S)(\mu_2\text{-}H)_2]$, $[(Cp^*IrH)_4(\mu_4\text{-}S)(\mu_2\text{-}H)_2]$, and $[(Cp^*Ir)_5Ir(\mu_3\text{-}S)_5H]$, were isolated from the reactions of $[(Cp^*Ir)_2(\mu_2\text{-}H)_3][BF_4]$ ($Cp^* = \eta^5\text{-}C_5Me_5$) with NaSH in MeOH. Treatment of **2** with $KOBu^t$ afforded the deprotonated product $[(Cp^*Ir)_3(\mu_3\text{-}S)(\mu\text{-}H)_2]$ (**7**), which was protonated by HBF_4 to give **2** reversibly. Addition of HBF_4 to **3** formed the dicationic cluster $[(Cp^*Ir)_4(\mu_3\text{-}S)_2(\mu\text{-}H)_2][BF_4]_2$ (**10**) with concurrent evolution of H_2, which was converted back to **3** under H_2 atmosphere in the presence of excess pyridine at 50 °C. In contrast, reactions of **10** with H_2 conducted in the presence of various alkylamines at 20–50 °C afforded the mixtures of **3** and its stereoisomer **11**. Conversion of **10** into **3** was also achieved by the reaction with 2 equiv of Cp_2Co in the presence of $[Et_3NH][BF_4]$, which furnished the cycle of reducing H^+ into H_2 mediated by the Ir_4S_2 cluster. Cluster **10** readily reacted with CO (1 atm) at 20 °C to give $[(Cp^*Ir)_4(\mu_3\text{-}S)_2(\mu\text{-}H)_2(CO)][BF_4]_2$ (**13**), where the CO ligand was bound in an end-on fashion to one of the two Ir centers connected to two μ_3-sulfido ligands. Analogous adduct formation was observed in the reaction of **10** with 1 equiv of XyNC (Xy = 2,6-dimethylphenyl), yielding two stereoisomers of $[(Cp^*Ir)_4(\mu_3\text{-}S)_2(\mu\text{-}H)_2(CNXy)][BF_4]_2$, one of which was the analogue of **13** and the other had the XyNC ligand coordinating to the same Ir site but with the inverted orientation around the metal. On the other hand, treatment of **10** with excess N_2H_4 gave the hydrazine cluster $[(Cp^*Ir)_4(\mu_3\text{-}S)_2(\mu_2\text{-}H)_2(N_2H_4)_2][BF_4]_2$, in which two terminal hydrazine ligands were bonded to one of two Ir sites supported by only one μ_3-sulfido ligand. On the basis of these findings about the adduct formations, reaction pathways of **10** with H_2 in the presence of bases are discussed. Structures of all new clusters reported here were determined by spectroscopic methods and, except for **7**, by X-ray crystallography.

Introduction

Metal sulfur clusters are known to play important roles in certain industrial and biological catalyses.[1] In these systems, activation and/or production of H_2 are involved as the key step. Thus, hydrodesulfurization of crude oil as a core process in the petroleum industry is catalyzed most commonly by the Co- or Ni-modified Mo sulfide, converting organosulfur compounds into hydrocarbons and H_2S through hydrogenolysis.[2] The active site is believed to consist of certain Co(Ni)−Mo mixed-metal sulfido clusters. On the other hand, in many microorganisms, reduction of protons to H_2 and its reverse reaction, separating H_2 into protons and electrons, are catalyzed by metalloenzymes called hydrogenases, whose active sites contain thiolato-bridged dinuclear Fe_2 or FeNi centers.[3] Nitrogen-fixing enzymes, nitrogenases, having a Fe_7MoS_9X (X = N, O, or C) mixed-metal sulfido cluster at their active site also function as hydrogenases, yielding not only ammonia but also H_2 gas by the uptake of protons and electrons.[4]

However, in spite of the recent rapid progress in the elucidation of the active site structures of these industrial and biological catalysts, detailed mechanisms operating at these sites for the activation and production of H_2 as well as the substrate reduction are yet uncertain. Preparation of transition-metal sulfido–hydrido clusters and clarification of the properties of their hydrido ligands as well as the reactivities of these clusters toward H_2 gas can therefore provide important information for understanding these catalyses[5,6] and lead potentially to the development of new hydrodesulfurization and hydrogen fuel technology. It is to be noted that although transition-metal hydrido complexes have been studied extensively as the key

* Corresponding author. E-mail: ymizobe@iis.u-tokyo.ac.jp.

(1) (a) Weber, T., Prins, R., van Santen, R. A., Eds. *Transition Metal Sulphides*; Kluwer Academic Publishers: Dordrecht, 1998. (b) Stiefel, E. I., Matsumoto, K., Eds. *Transition Metal Sulfur Chemistry: Biological and Industrial Significance*; American Chemical Society: Washington, DC, 1996. (c) Rees, D. C. *Annu. Rev. Biochem.* **2002**, *71*, 221.

(2) (a) Startsev, A. N. *J. Mol. Catal. A* **2000**, *152*, 1. (b) Kabe, T.; Ishihara, A.; Qian, W. *Hydrodesulfurization and Hydrodenitrogenation*; Kodansha Ltd. and Wiley-VHC: Tokyo, 1999. (c) Topsøe, H.; Clausen, B. S.; Massoth, F. E. In *Catalysis: Science and Technology*; Anderson, J. R., Boudart, M.,Eds.; Springer-Verlag: Berlin, Vol. 11, 1996. (d) Chianelli, R. R.; Daage, M.; Ledoux, M. J. *Adv. Catal.* **1994**, *40*, 177.

(3) (a) *Coord. Chem. Rev.* **2005**, *249*, issues 15–16. (b) Vincent, K. A.; Cracknell, J. A.; Parkin, A.; Armstrong, F. A. *Dalton Trans.* **2005**, 3397. (c) Volbeda, A.; Fontecilla-Camps, J. C. *Dalton Trans.* **2003**, 4030. (d) Evans, D. J.; Pickett, C. J. *Chem. Soc. Rev.* **2003**, *32*, 268.

(4) (a) Burgess, B. K.; Lowe, D. J. *Chem. Rev.* **1996**, *96*, 2983. (b) Thorneley, R. N. F.; Lowe, D. J. *J. Biol. Inorg. Chem.* **1996**, *1*, 576. (c) Sellmann, D.; Fürsattel, A.; Sutter, J. *Coord. Chem. Rev.* **2000**, *200–202*, 545. (d) Igarashi, R. Y.; Laryukhin, M.; Dos Santos, P. C.; Lee, H.-I.; Dean, D. R.; Seefeldt, L. C.; Hoffman, B. M. *J. Am. Chem. Soc.* **2005**, *127*, 6231.

(5) (a) Clusters for hydrodesulfurization model: Brorson, M.; King, J. D.; Kiriakidou, K.; Prestopino, F.; Nordlander, E. In *Metal Clusters in Chemistry*; Braunstein, P., Oro, L. A., Raithby, P. R. Eds.; Wiley-VHC: Weinheim, 1999; Chapter 2.6. (b) Curtis, M. D.; Druker, S. H. *J. Am. Chem. Soc.* **1997**, *119*, 1027. (c) Rakowski Dubois, M. *Polyhedron* **1997**, *16*, 3089. (d) Angelici, R. J. *Polyhedron* **1997**, *16*, 3073. (e) Curtis, M. D. In *Transition Metal Sulfur Chemistry: Biological and Industrial Significance*; Stiefel, E. I., Matsumoto, K., Eds.; American Chemical Society: Washington, DC, 1996; Chapter 8. (f) Wiegand, B. C.; Friend, C. M. *Chem. Rev.* **1992**, *92*, 491.

10.1021/om701207j CCC: $40.75
Publication on Web 02/21/2008

intermediates in catalytic homogeneous hydrogenation,[7] chemistry of the hydrido-sulfido clusters is still poorly advanced.[8,9]

Our recent research has focused on syntheses of transition-metal sulfido clusters and exploration of their reactivities to activate small molecules effectively.[10–15] For the systems using metal sulfido clusters, it may be expected that reaction proceeds with retention of their multimetallic core structures even under relatively forcing conditions, owing to the presence of firmly bonded sulfido bridges. In this paper, we wish to describe the structures and reactivities of a series of new Ir sulfido clusters having hydrido ligands, which have been synthesized from the reactions of the Ir hydrido complex $[(Cp^*Ir)_2(\mu\text{-}H)_3][BF_4]$ (**1**; $Cp^* = \eta^5\text{-}C_5Me_5$) with controlled amount of the sulfido source. Interestingly, the features of the hydrido ligands in these clusters vary significantly from *hydridic* to *protic*, as demonstrated by their reactivities toward acids and bases. The factors determining their features are also discussed.

Results and Discussion

Preparation of the Sulfido-Hydrido Clusters of Iridium. When 0.67 equiv of NaSH was added slowly (over >5 h) to a MeOH solution of **1** at room temperature, a mixture of several Ir sulfido–hydrido clusters was formed (Scheme 1). Two major products from this reaction of Ir/S = 3 are the cationic triiridium cluster $[(Cp^*Ir)_3(\mu_3\text{-}S)(\mu_2\text{-}H)_3][BF_4]$ (**2**) and the tetrairidium cluster $[(Cp^*Ir)_4(\mu_3\text{-}S)_2(\mu_2\text{-}H)_3][BF_4]$ (**3**), which are both soluble in MeOH and were isolated as red and dark reddish-brown crystals, respectively, after the workup of the filtrate of the reaction mixture. The yield of the former was 32%, while that of the latter was 17%, based on the Ir charged. Two neutral clusters as minor products, $[(Cp^*IrH)_2(Cp^*Ir)(\mu_3\text{-}S)(\mu_2\text{-}H)_2]$ (**4**) and $[(Cp^*IrH)_4(\mu_4\text{-}S)(\mu_2\text{-}H)_2]$ (**5**), were also obtained as dark red and orange crystals, respectively, in quite low yields by recrystallizing a small amount of solid precipitated from the reaction mixture. Clusters **2**–**5** were characterized by spectroscopic and elemental analysis data as well as X-ray crystallography (vide infra).

Scheme 1

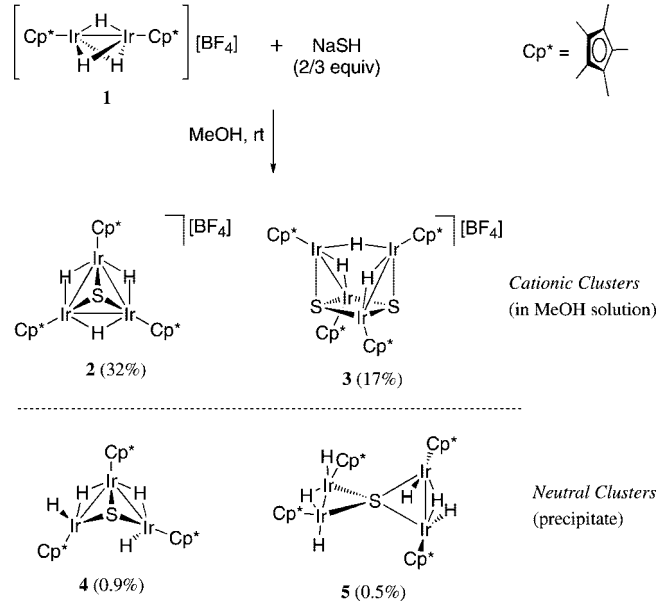

Yields based on Ir are in parentheses.

To improve the yield of **3**, the reaction of equimolar amounts of **1** and NaSH, viz., Ir/S = 2, was attempted. This resulted in the expected decrease in the yield of **2** (ca. 3%), but the yield of **3** increased only slightly (18–22%) regardless of the addition rate of NaSH (Scheme 2). On the other hand, two new clusters were also obtained as the products from this reaction mixture. One is the neutral hexairidium cluster $[(Cp^*Ir)_5Ir(\mu_3\text{-}S)_5H]$ (**6**), which was isolated as dark green crystals in low yield (1.5%) and fully characterized. The other is another neutral cluster tentatively formulated as $[(Cp^*Ir)_3(\mu_3\text{-}S)(\mu\text{-}H)_2]$ (**7**), which was present as the major component in the benzene extract from the evaporated residue of the filtrate of the reaction mixture, but its very high solubility in common organic solvents prevented further purification. By treatment with HBF_4 in MeOH, **7** present in the benzene extract was converted to the well-defined **2**, which was isolated in 37% yield based on **1**. From this acidified mixture of benzene extract, cationic sulfido clusters with no hydrido ligands, $[(Cp^*Ir)_3(\mu_3\text{-}S)_2][BF_4]_2$ (**8**)[16] and $[(Cp^*Ir)_4Ir(\mu_3\text{-}S)_4][BF_4]_3$ (**9**),[17] were also obtained in ca. 4% combined yield. Thus, the increase in the molar ratio NaSH/**1** from 0.67 to 1 resulted in the formation of **7** instead of **2** in significant yield as well as the production of relatively sulfur-rich clusters **6**, **8**, and **9** despite their low yields.

(6) (a) Complexes for hydrogenase model: Tard, C.; Liu, X.; Ibrahim, S. K.; Bruschi, M.; De Gioia, L.; Davies, S. C.; Yang, X.; Wang, L.-S.; Sawers, G.; Pickett, C. J. *Nature* **2005**, *433*, 610. (b) van der Vlugt, J. I.; Rauchfuss, T. B.; Whaley, C. M.; Wilson, S. R. *J. Am. Chem. Soc.* **2005**, *127*, 16012. (c) Li, Z.; Ohki, Y.; Tatsumi, K. *J. Am. Chem. Soc.* **2005**, *127*, 8950. (d) Mejia-Lodriguez, R.; Chong, D.; Reibenspies, J. H.; Soriaga, M. P.; Darensbourg, M. Y. *J. Am. Chem. Soc.* **2004**, *126*, 12004.

(7) (a) Humphries, A. P.; Kaesz, H. D. *Prog. Inorg. Chem.* **1979**, *25*, 145. (b) Plasseraud, L.; Süss-Fink, G. *J. Organomet. Chem.* **1997**, *539*, 163. (c) Ferrand, V.; Süss-Fink, G.; Neels, A.; Stoeckli-Evans, H. *J. Chem. Soc., Dalton Trans.* **1999**, 3825. (d) Nagashima, H. *Monatsh. Chem.* **2000**, *131*, 1225. (e) Süss-Fink, G.; Faure, M.; Ward, T. R. *Angew. Chem., Int. Ed.* **2002**, *41*, 99. (f) Adams, R. D.; Captain, B. *J. Organomet. Chem.* **2004**, *689*, 4521. (g) Adams, R. D.; Captain, B.; Zhu, L. *J. Am. Chem. Soc.* **2004**, *126*, 3042.

(8) (a) Reactions of sulfido clusters with H_2: Adams, R. D.; Wang, S. *Organometallics* **1986**, *5*, 1272. (b) Adams, R. D.; Babin, J. E.; Tasi, M.; Wolfe, T. A. *New J. Chem.* **1988**, *12*, 481. (c) Vaartstra, B. A.; Cowie, M. *Inorg. Chem.* **1989**, *28*, 3138. (d) Matsubara, K.; Inagaki, A.; Tanaka, M.; Suzuki, H. *J. Am. Chem. Soc.* **1999**, *121*, 7421. (e) Ohki, Y.; Matsuura, N.; Marumoto, T.; Kawaguchi, H.; Tatsumi, K. *J. Am. Chem. Soc.* **2003**, *125*, 7978. (f) Takei, I.; Suzuki, K.; Enta, Y.; Dohki, K.; Suzuki, T.; Mizobe, Y.; Hidai, M. *Organometallics* **2003**, *22*, 1790. (g) Justice, A. K.; Linck, R. C.; Rauchfuss, T. B.; Wilson, S. R. *J. Am. Chem. Soc.* **2004**, *126*, 13214. (h) Tschan, M.; Therrien, B.; Chérioux, F.; Süss-Fink, G. *J. Mol. Struct.* **2005**, *743*, 177. (i) Takei, I.; Kobayashi, K.; Dohki, K.; Nagao, S.; Mizobe, Y.; Hidai, M. *Chem. Lett.* **2007**, *36*, 546.

(9) (a) Interactions of H_2 with μ-sulfido ligands in certain dinuclear complexes: Casewit, C. J.; Coons, D. E.; Wright, L. L.; Müller, W. K.; Rakowski DuBois, M. *Organometallics* **1986**, *5*, 951. (b) Laurie, J. C. V.; Duncan, L.; Haltiwanger, R. C.; Weberg, R. T.; Rakowski DuBois, M. *J. Am. Chem. Soc.* **1986**, *108*, 6234. (c) Bianchini, C.; Mealli, C.; Meli, A.; Sabat, M. *Inorg. Chem.* **1986**, *25*, 4618. (f) Linck, R. C.; Pafford, R. J.; Rauchfuss, T. B. *J. Am. Chem. Soc.* **2001**, *123*, 8856. (g) Kato, H.; Seino, H.; Mizobe, Y.; Hidai, M. *J. Chem. Soc., Dalton Trans.* **2002**, 1494. (h) Ienco, A.; Calhorda, M. J.; Reinhold, J.; Reineri, F.; Bianchini, C.; Peruzzini, M.; Vizza, F.; Mealli, C. *J. Am. Chem. Soc.* **2004**, *126*, 11954.

(10) (a) Masumori, T.; Seino, H.; Mizobe, Y.; Hidai, M. *Inorg. Chem.* **2000**, *39*, 5002. (b) Seino, H.; Masumori, T.; Hidai, M.; Mizobe, Y. *Organometallics* **2003**, *22*, 3424.

(11) (a) Takagi, F.; Seino, H.; Hidai, M.; Mizobe, Y. *Organometallics* **2003**, *22*, 1065. (b) Kajitani, H.; Seino, H.; Mizobe, Y. *Organometallics* **2005**, *24*, 6260.

(12) Yoshizawa, K.; Kihara, N.; Shiota, Y.; Seino, H.; Mizobe, Y. *Bull. Chem. Soc., Jpn.* **2006**, *79*, 53.

(13) Saito, A; Seino, H.; Kajitani, H.; Takagi, F.; Yashiro, A.; Ohnishi, T.; Mizobe, Y. *J. Organomet. Chem.* **2006**, *691*, 5746.

(14) Kajitani, H.; Seino, H.; Mizobe, Y. *Organometallics* **2007**, *26*, 3499.

(15) Mori, H.; Seino, H.; Hidai, M.; Mizobe, Y. *Angew. Chem., Int. Ed.* **2007**, *46*, 5431.

(16) Nishioka, T.; Isobe, K. *Chem. Lett.* **1994**, 1661.

(17) Atom connecting scheme was confirmed by preliminary X-ray analysis. Crystallographic data are as follows: monoclinic, space group $P2_1/n$, $a = 18.041(7)$ Å, $b = 14.385(5)$ Å, $c = 21.616(8)$ Å, $\beta = 108.472(2)°$, $V = 5321(3)$ Å^3, $Z = 4$.

Scheme 2

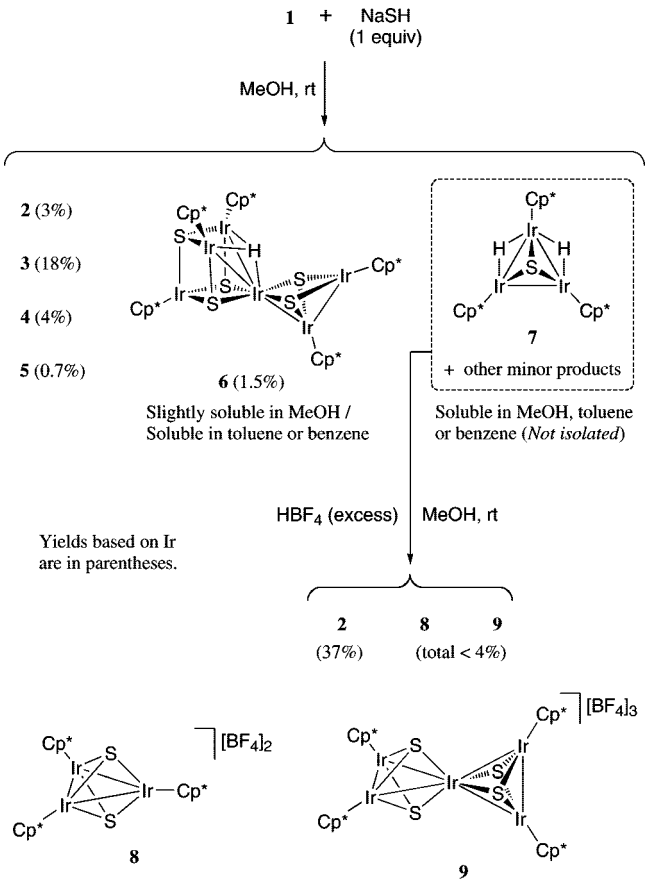

It might also be noteworthy that the reaction of **1** with NaSH in MeCN in place of MeOH gave a complicated mixture containing some uncharacterizable products in addition to **2–5**, whereas with the use of Na_2S as the sulfur source the major product of the reaction became the hydrido complex $[(Cp^*Ir)_2(\mu_2\text{-}H)_2]$.[18]

Characterization of the Clusters 2–6. The hydrido-sulfido clusters **2–6** have been characterized by combination of spectroscopic data and single-crystal X-ray diffraction studies as follows. The structure of the cationic part of **2** is shown in Figure 1. It has a triangular Ir_3 core capped by one μ_3-sulfido ligand, and each Cp* ligand orients almost perpendicularly to the Ir_3 plane with deviations less than 2°. The Ir−Ir distances in the range 2.8619(7)–2.8638(6) Å are mutually in good agreement and the Ir−S bond lengths are also essentially identical (2.299(3)–2.305(3) Å), indicating the cation has pseudo-C_{3v} symmetry in spite of the lack of any crystallographically imposed symmetry. The ^{1}H NMR spectrum of **2** in $CDCl_3$ shows one signal assignable to Cp* ligands at δ 2.24 as well as one singlet due to the hydrido ligands at δ −21.86 in a ratio of 15:1, which suggests the existence of one hydrido ligand per one Cp*Ir fragment. It seems reasonable to assume that three hydrido ligands bridge three Ir−Ir edges, and this has been confirmed by the appearance of three H atoms at the expected positions in the Fourier map (Ir−H, 1.7(1)–1.9(1) Å; Ir−H−Ir, 101(6)–117(7)°; S−Ir−H, 82(4)–91(3)°; H−Ir−H, 76(5)–81(5)°). Therefore, short Ir−Ir distances in **2** are attributable to the three-centered−two-electron bonds involving μ_2-hydrido ligands. These bonds are longer than the Rh−Rh distances in the homologous oxo cluster $[(Cp^*Rh)_3(\mu_3\text{-}O)(\mu_2\text{-}H)_3][PF_6]$ at 2.755(1)–2.770(1) Å[19] but only slightly longer than the Ir−Ir single bonds in the triangular Ir_3 bis(sulfido) clusters, such as **8** and its PF_6^- salt (2.832(1) and 2.8157(7)–2.8201(7) Å, respectively),[16,20] and analogous to those in the other Cp*Ir complexes having mono-μ_2-hydrido bridged Ir−Ir moieties, e.g., $[(Cp^*IrCl)_2(\mu_2\text{-}SR)(\mu_2\text{-}H)]$ (R = Bu, 2-ethylphenyl, $(\eta^3\text{-}C_3H_3Me)IrCp^*Cl$) at 2.8859(4)–2.9139(3) Å,[21] $[(Cp^*IrCl)_2(\mu_2\text{-}Cl)(\mu_2\text{-}H)]$ at 2.903(1) Å,[22] $[\{Cp^*Ir(CO)\}_2(\mu_2\text{-}CO)(\mu_2\text{-}H)][OTf]$ (OTf = CF_3SO_3) at 2.831(1) Å,[23] $[\{Cp^*Ir(Ph)\}(\mu_2\text{-}\eta^1,\eta^3\text{-}C_3H_4)(\mu_2\text{-}H)(IrCp^*)]$ at 2.867(1) and 2.872(1) Å,[24] $[(Cp^*Ir)_2(\mu_2\text{-}dmpm)(\mu_2\text{-}L)(\mu_2\text{-}H)][OTf]_2$ (dmpm = $Me_2PCH_2PMe_2$; L = η^1,η^2-CBu=CH_2, η^1,η^2-CH=CHPh, CNHPh) at 2.855(1)–2.9329(6) Å,[25] and $[(Cp^*Ir)_2(\mu_2\text{-}PPh_2)(\mu_2\text{-}C_6H_4)(\mu_2\text{-}H)]$ at 2.8901(4) Å.[26] The Ir−S distances in **2** are almost comparable to those in **8** (2.289(3) Å for BF_4 salt and 2.275(3)–2.294(3) Å for PF_6 salt).

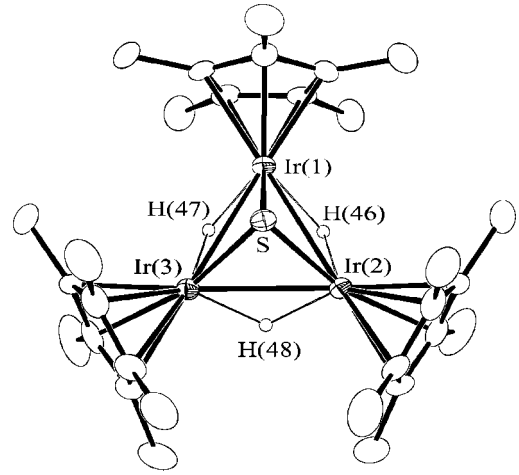

Figure 1. Molecular structure of the cationic part of **2** (thermal ellipsoids at the 30% probability level). Hydrogen atoms in Cp* ligands are omitted for clarity. Bond distances (Å) and angles (deg): Ir(1)−Ir(2), 2.8638(6); Ir(1)−Ir(3), 2.8625(7); Ir(2)−Ir(3), 2.8619(7); Ir(1)−S, 2.305(3); Ir(2)−S, 2.299(3); Ir(3)−S, 2.301(3); Ir(2)−Ir(1)−Ir(3), 59.97(2); Ir(1)−Ir(2)−Ir(3), 59.99(2); Ir(1)−Ir(3)−Ir(2), 60.04(2); Ir(1)−S−Ir(2), 76.92(9); Ir(1)−S−Ir(3), 76.85(9); Ir(2)−S−Ir(3), 76.94(9).

The cationic part of **3** depicted in Figure 2 has a distorted trigonal-prismatic Ir_4S_2 core, which is defined by the Ir(1)−Ir(2)−S and Ir(1*)−Ir(2*)−S* basal planes connected each other by the Ir(2)−Ir(2*), Ir(1)−S*, and S−Ir(1*) edges. A crystallographic 2-fold axis passes through the midpoint of the Ir(1)−Ir(1*) and Ir(2)−Ir(2*) vectors. The Ir(1) atom is connected to two μ_3-sulfido ligands S and S*, while the Ir(2) is bonded to only the S atom. Thus, two ^{1}H NMR signals of Cp* ligands appear at δ 1.97 and 2.03 in $CDCl_3$ at 20 °C corresponding to the inequivalent Ir centers. There are two more proton signals at δ −25.34 and −15.02, which are observed as a triplet and a

(18) Hou, Z.; Fujita, A.; Koizumi, T.; Yamazaki, H.; Wakatsuki, Y. *Organometallics* **1999**, *18*, 1979.

(19) Nutton, A.; Bailey, P. M.; Braund, N. C.; Goodfellow, R. J.; Thompson, R. S.; Maitlis, P. M. *J. Chem. Soc., Chem. Commun.* **1980**, 631.

(20) Venturelli, A.; Rauchfuss, T. B. *J. Am. Chem. Soc.* **1994**, *116*, 4824.

(21) Vicic, D. A.; Jones, W. D. *Organometallics* **1997**, *16*, 1912.

(22) Churchill, M. R.; Julis, S. A. *Inorg. Chem.* **1977**, *16*, 1488.

(23) Heinekey, D. M.; Fine, D. A.; Barnhart, D. *Organometallics* **1997**, *16*, 2530.

(24) McGhee, W. D.; Hollander, F. J.; Bergman, R. G. *J. Am. Chem. Soc.* **1988**, *110*, 8428.

(25) Fujita, K.; Nakaguma, H.; Hanasaka, F.; Yamaguchi, R. *Organometallics* **2002**, *21*, 3749.

(26) Grushin, V. V.; Vymenits, A. B.; Yanovsky, A. I.; Struchkov, Y. T.; Vol'pin, M. E. *Organometallics* **1991**, *10*, 48.

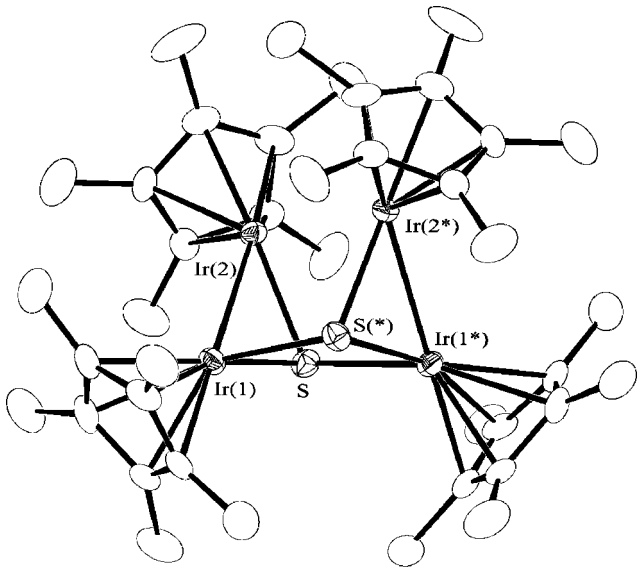

Figure 2. Molecular structure of the cationic part of **3** (thermal ellipsoids at the 30% probability level). Hydrogen atoms are omitted for clarity. Interatomic distances (Å) and bond angles (deg): Ir(1)−Ir(2), 2.8662(7); Ir(1)···Ir(1*), 3.6036(8); Ir(1)···Ir(2*), 3.8104(8); Ir(2)···Ir(2*), 3.1757(7); Ir(1)−S, 2.320(3), Ir(1)−S(*), 2.345(4); Ir(2)−S, 2.323(4); S−Ir(1)−S(*), 77.9(1); Ir(1)−S−Ir(2), 76.2(1); Ir(1)−S−Ir(1*), 101.1(1); Ir(1*)−S−Ir(2), 109.4(1).

doublet integrated to be 1H and 2H, respectively, and coupled to each other with $J \approx 2$ Hz. The former signal is presumably assignable to the hydrido ligand bridging the Ir(2)−Ir(2*) edge, and the latter is assignable to those at the Ir(1)−Ir(2) and Ir(1*)−Ir(2*) edges, although they could not be located in the difference Fourier map. By the presence of these hydrido ligands, both Ir(1) and Ir(2) centers adopt three-legged piano-stool geometries if Ir−Ir interactions are neglected. The Ir(1)−Ir(2) distance at 2.8662(7) Å is typical for three-centered−two-electron Ir−H−Ir bonding as found in **2**. In contrast, the Ir(2)−Ir(2*) distance at 3.1757(7) Å is considerably elongated probably due to the steric repulsion between the Cp* ligands attached to these Ir atoms. Similar long Ir−Ir bonds with μ_2-hydrido bridges have been found in some complexes such as $[(Tp^{Me2}IrH)_2(\mu_2\text{-}\eta^1,\eta^1\text{-}C,S\text{-}C_4H_3S)(\mu_2\text{-H})]$ (Tp^{Me2} = $HB(3,5\text{-}Me_2C_3HN_2)_3$) at 3.066(1) Å,[27] $[(Cp^*Ir)_2(\mu_2\text{-}\eta^1,\eta^1\text{-}4\text{-methyl-1-pyrazolyl})_2(\mu_2\text{-H})][PF_6]$ at 3.0670(4) Å,[28] and $[\{Cp^*Ir(CNBu^t)\}(\mu_2\text{-dmpm})(\mu_2\text{-H})\{IrCp^*(H)\}][OTf]_2$ at 3.168(1) Å.[25] Other Ir···Ir distances in **3** longer than 3.6 Å indicate the absence of any Ir−Ir bonding interactions or bridging hydrido ligands there, which is consistent with the cluster electron count of 66 bearing three Ir−Ir single bonds bridged by μ_2-H ligands. The Ir−S bond distances at 2.320(3)–2.345(4) Å are slightly longer than those in **2** but not unusual for the Cp*Ir(III)-(μ_3-sulfido) single bonds, e.g., $[(Cp^*Ir)_4(\mu_3\text{-S})_4]$ at 2.367(3)–2.380(3) Å[29] and $[(Cp^*Ir)_2(Cp^{\#}Ru)(\mu_3\text{-S})(\mu_2\text{-}SCH_2CH_2CN)(L)]^+$ ($Cp^{\#}$ = Cp*, η^5-C_5H_5 (Cp); L = Cl^-, CO, CNXy (Xy = 2,6-dimethylphenyl)) at 2.369(1)–2.414(1) Å.[11]

The structure of the neutral trinuclear cluster **4** is depicted in Figure 3, whose core consists of a nearly isosceles Ir_3 triangle capped by a μ_3-sulfido ligand from one side. All four hydrido

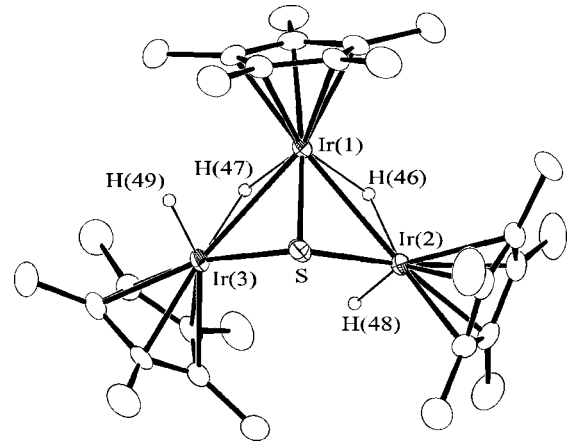

Figure 3. Molecular structure of **4** (thermal ellipsoids at the 30% probability level). Hydrogen atoms in Cp* ligands are omitted for clarity. Interatomic distances (Å) and bond angles (deg): Ir(1)−Ir(2), 2.8770(5); Ir(1)−Ir(3), 2.8665(6); Ir(2)···Ir(3), 3.7530(5); Ir(1)−S, 2.302(2); Ir(2)−S, 2.313(2); Ir(3)−S, 2.317(2); Ir(2)−Ir(1)−Ir(3), 81.60(2); Ir(1)−S−Ir(2), 77.13(6); Ir(1)−S−Ir(3), 76.72(6); Ir(2)−S−Ir(3), 108.3(1).

ligands were located in the difference Fourier map and successfully refined with isotropic parameters (Ir−H at 1.5(1)–1.84(9) Å and Ir−H−Ir at 105(5)°, 113(4)°). Two μ_2-H ligands bridge the Ir(1)−Ir(2) and Ir(1)−Ir(3) edges, whose distances are 2.8770(5) and 2.8665(6) Å, respectively. In addition, there is a terminal hydrido ligand on each of the Ir(2) and Ir(3) atoms, which is confirmed by the IR bands at 2148 and 2104 cm^{-1}, characteristic of the Ir−H stretching mode. Separation between Ir(2) and Ir(3) atoms at 3.7530(5) Å indicates the absence of bonding interaction in accordance with the cluster electron count of 50. If Ir−Ir bonds are excluded from consideration, each Ir center adopts three-legged piano-stool geometry with S−Ir−H and H−Ir−H angles at 78(2)–89(3)° and 78(6)–86(5)°, respectively. The Cp* ligands coordinated to Ir(1) and Ir(2) are oriented mutually cis with respect to the Ir(1)Ir(2)SH(46) moiety. In contrast, the Cp* ligands bound to Ir(1) and Ir(3) are located mutually at the opposite sides of the Ir(1)Ir(3)SH(47) plane. Among four hydride ligands in **4**, only the terminal H(49) bonded to the Ir(3) atom exists on the same side of the μ_3-sulfide with respect to the Ir_3 plane, while the other three are on the opposite side.

The ^{1}H NMR spectrum of **4** in THF-d_8 at −20 °C exhibits three inequivalent Cp* and four distinct hydrido proton signals (δ –20 to −15), being consistent with the crystal structure lacking any molecular symmetry. When the temperature was raised to 55 °C, fusion of two of the three Cp* signals and considerable broadening of all the hydride signals occurred. Spin saturation-transfer experiments at 30 °C confirmed that exchange of the hydrido ligands occurred only within each of two pairs (between the signals at δ −15.60 and −19.87 and those at δ −17.53 and −19.92) and not across these pairs. This fluxional behavior is likely to correspond to the motion dipicted in Scheme 3, where two terminal Cp^*IrH_2 moieties concertedly rotate around the Ir−S axes under retention of the geometries around the Ir centers. The activation parameters of this motion has been estimated to be $\Delta H^{\ddagger} = 63 \pm 1$ kJ mol^{-1} and $\Delta S^{\ddagger} = -12 \pm 4$ J mol^{-1} K^{-1}, based on line-shape analysis of the Cp* signals.

The tetranuclear cluster **5** has the core structure where a μ_4-sulfido ligand assembles two diiridium subunits as shown in Figure 4. Two Cp*Ir centers in a subunit are separated by 2.8497(4) and 2.8437(6) Å, and the Cp* ligands bound to them

(27) Paneque, M.; Poveda, M. L.; Salazar, V.; Taboada, S.; Carmona, E.; Gutiérrez-Puebla, E.; Monge, A.; Ruiz, C. *Organometallics* **1999**, *18*, 139.
(28) Faure, M.; Onidi, A.; Neels, A.; Stoeckli-Evans, H.; Süss-Fink, G. *J. Organomet. Chem.* **2001**, *634*, 12.
(29) Dobbs, D. A; Bergman, R. G. *Inorg. Chem.* **1994**, *33*, 5329.

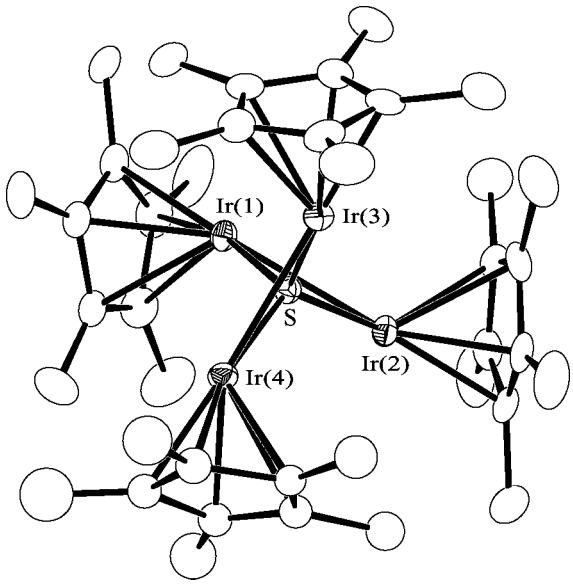

Figure 4. Molecular structure of **5** (thermal ellipsoids at the 30% probability level). Hydrogen atoms and the minor conformer of the disordered Cp* ligand bound to Ir(4) are omitted for clarity. Bond distances (Å) and angles (deg): Ir(1)−Ir(2), 2.8497(4); Ir(3)−Ir(4), 2.8437(6); other Ir···Ir, 4.1368(4)–4.1621(4); Ir(1)−S, 2.300(2); Ir(2)−S, 2.303(2); Ir(3)−S, 2.306(2); Ir(4)−S, 2.309(2); Ir(1)−S−Ir(2), 76.49(5); Ir(1)−S−Ir(3), 128.19(9); Ir(1)−S−Ir(4), 127.7(1); Ir(2)−S−Ir(3), 128.0(1); Ir(2)−S−Ir(4), 128.96(9); Ir(3)−S−Ir(4), 76.08(5).

Scheme 3

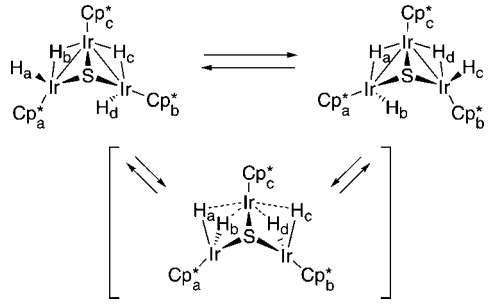

are oriented mutually to the opposite sides with respect to the Ir_2S plane. The dihedral angle at 89° between two Ir_2S triangles makes the intersection of these planes a pseudo-S_4 axis, which is consistent with the observation that the ^{1}H NMR signal of four Cp* ligands appears as one singlet. Hydride resonances are observed as a doublet at δ −17.37 and a triplet at δ −19.06 with the intensities of 4H and 2H, respectively, and these are mutually coupling with $J \approx 3$ Hz. The IR absorption at 2080 cm^{-1} suggests the existence of terminal hydrido ligands. According to the molecular symmetry, it may be assumed that each Ir atom has a terminal hydrido ligand and that each Ir_2 subunit has a bridging hydride lying on the pseudo-S_4 axis. It is inferred from the conformation of the Cp* ligands that two terminal hydrides in a subunit are present at the opposite sides of the Ir_2S plane to each other. Such orientation of the hydrido ligands is observed in $[\{Cp^*IrH(PMe_3)\}_2(\mu_2\text{-}H)][PF_6]$[30] and $[(Cp^*Ir)_2(H)_3(BH_4)]$.[31]

Figure 5 shows the crystal structure of **6**. The molecule is regarded to consist of five Cp*Ir(III) fragments and one Ir(I) center together with five μ_3-sulfido and one hydrido ligands. The cluster core is built up from an Ir_4 tetrahedron (Ir(1)−Ir(4)) and an Ir_3 triangle (Ir(1), Ir(5), and Ir(6)), sharing the Ir(1) vertex without the Cp* coligand. Three of four faces of the former Ir_4

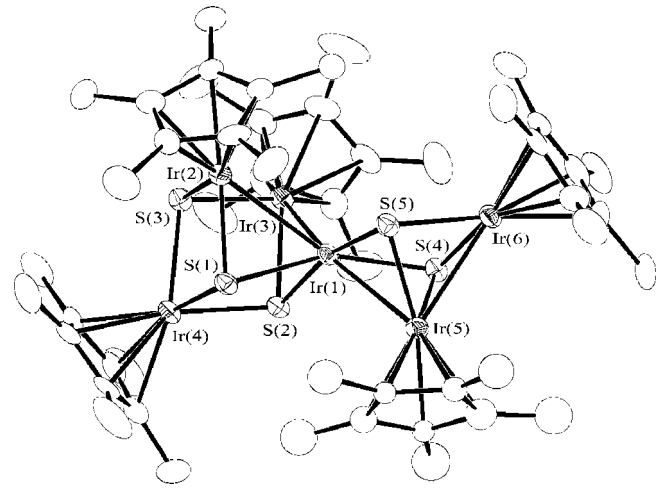

Figure 5. Molecular structure of **6** (thermal ellipsoids at the 30% probability level). Hydrogen atoms and the minor conformer of the disordered Cp* ligand bound to Ir(5) are omitted for clarity. Bond distances (Å) and angles (deg): Ir(1)−Ir(2), 2.8745(8); Ir(1)−Ir(3), 2.8667(6); Ir(1)−Ir(5), 2.7044(7); Ir(5)−Ir(6), 2.7825(9); Ir(1)···Ir(4), 3.5902(6); Ir(1)···Ir(6), 3.5704(6); Ir(2)···Ir(3), 3.5282(6); Ir(2)···Ir(4), 3.5463(7); Ir(3)···Ir(4), 3.5958(8); Ir(1)−S(1), 2.377(4); Ir(1)−S(2), 2.375(3); Ir(1)−S(4), 2.343(4); Ir(1)−S(5), 2.342(3); Ir(2)−S(1), 2.282(4); Ir(2)−S(3), 2.347(3); Ir(3)−S(2), 2.338(4); Ir(3)−S(3), 2.358(4); Ir(4)−S, 2.372(3)–2.375(4); Ir(5)−S, 2.315(3), 2.329(4); Ir(6)−S, 2.295(4), 2.312(3); S(1)−Ir(1)−S(2), 80.3(1); S(1)−Ir(1)−S(4), 156.0(1); S(1)−Ir(1)−S(5), 100.7(1); S(2)−Ir(1)−S(4), 96.7(1); S(2)−Ir(1)−S(5), 167.2(1); S(4)−Ir(1)−S(5), 77.1(1); S(1)−Ir(2)−S(3), 82.2(1); S(2)−Ir(3)−S(3), 80.8(1); S−Ir(4)−S, 79.8(1)–80.4(1); S(4)−Ir(5)−S(5), 77.9(1); S(4)−Ir(6)−S(5), 78.7(1).

subunit are capped by μ_3-sulfido ligands, and the shared Ir(1) atom resides at the uncapped face. This unit possesses a pseudomirror plane passing through atoms Ir(1), Ir(4), and S(3). Two more μ_3-sulfides symmetrically cover both sides of the latter Ir_3 triangle, which is twisted by 9.4° against the pseudomirror plane of the Ir_4 unit. Four sulfur atoms bonded to the Ir(1) center are slightly deviated from planarity, and Ir(1) is apart from that least-squares plane by 0.37 Å toward the opposite side of Ir(5). The ^{1}H NMR spectrum of **6** in solution showing four signals assignable to the Cp* ligands in 1:1:1:2 intensity ratio indicates that the cluster has a C_s-symmetry where Ir(2) and Ir(3) are equivalent. One hydrido ligand, which appears at δ −13.31, exists probably somewhere on the Ir(1)Ir(2)Ir(3) face, although its crystallographic determination has been unsuccessful. The number of four intermetallic bonds in the cluster agrees with a 100 electron count.

Interconversion among Trinuclear Sulfido-Hydrido Clusters. As described above, although **7** was formed in the reaction of **1** with an equimolar amount of NaSH in moderate yield, isolation in a pure form was unsuccessful. However, since it has turned out that **7** is treated with HBF_4 to be converted into well-defined **2**, reaction of **2** with base was attempted. Thus, when treated with excess $KOBu^t$ in THF at room temperature, **2** was transformed back to **7** cleanly as expected, which was isolated in high yield in pure form. The ^{1}H NMR spectrum of **7** in C_6D_6 shows two singlets at δ 2.16 and −20.98 assignable to three Cp* and two hydrido ligands, respectively, and no IR

(30) (a) Gilbert, T. M.; Bergman, R. G. *J. Am. Chem. Soc.* **1985**, *107*, 3502. (b) Burns, C. J.; Rutherford, N. M.; Berg, D. J. *Acta Crystallogr. Sect. C* **1987**, *C43*, 229.

(31) Gilbert, T. M.; Hollander, F. J.; Bergman, R. G. *J. Am. Chem. Soc.* **1985**, *107*, 3508.

Scheme 4

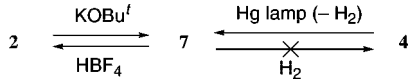

bands assignable to the terminal Ir−H bonds are observed in the region of 1800–2500 cm^{-1}. The IR spectrum also indicates the absence of BF_4^- anion, and its high solubility in nonpolar solvents is consistent with the neutral character. On the basis of these findings, the structure of **7** may be characterized to be that obtained by the elimination of one of three hydrido ligands in **2** as a proton, as shown in Scheme 2. Presumably, two hydrido ligands in **7** are both present at the Ir−Ir edges, or one is at the Ir_3 face and the other is at the Ir−Ir edge, which are rapidly migrating even at −70 °C, since three Cp* ligands are equivalently observed in the ^{1}H NMR spectrum.

Formation of **7** was also observed on UV irradiation of a C_6D_6 solution of **4** through dehydrogenation, although the reaction was quite slow at room temperature (50% conversion after 18 h) and afforded byproduct to some extent. On the other hand, reaction of **7** with H_2 does proceed only under drastic conditions (50 atm, 110 °C), yielding no **4** at all but Cp^*IrH_4[31] together with uncharacterized hydrido species. Transformation of these triiridium-monosulfide clusters is summarized in Scheme 4. Interconversion between 48-electron clusters **2** and **7** is reversible, accompanied by the change in the formal oxidation states between $Ir(III)_3$ and $Ir(II)_2Ir(III)$, respectively. Attempts to prepare the 50-electron cluster **4** from **2** by hydride reduction also failed.

Interconversion among Tetranuclear Sulfido-Hydrido Clusters. The cationic triiridium cluster **2** was not amenable to further protonation, whereas tetrairidium cluster **3** readily reacted with HBF_4 to give the dicationic cluster $[(Cp^*Ir)_4(\mu_3\text{-}S)_2(\mu\text{-}H)_2][BF_4]_2$ (**10**) in high yield (eq 1). In the course of this reaction, concomitant evolution of H_2 (0.67–0.76 equiv of **3**) was observed. The ^{1}H NMR spectrum of **10** showed two Cp* signals, each integrated for 30H and a singlet for two hydrido ligands. Single-crystal X-ray analysis has revealed the details of the molecular structure of **10**, whose cationic part is shown in Figure 6. The cluster consists of an Ir_4 tetrahedron, with two μ_3-sulfido ligands capping two faces. The Ir atoms are classified into two types: those bound to two S atoms (Ir(1) and Ir(2)) and those bound with only one Ir−S bond (Ir(3) and Ir(4)), as observed in the parent cluster **3**. These Ir atoms are denoted as Ir(α) and Ir(β), respectively, for any Ir_4S_2 clusters below throughout this article.

The Ir_4S_2 framework of **10** possesses two pseudomirror

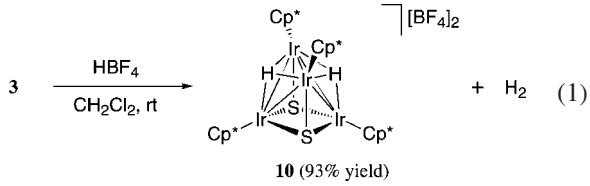

planes, one of which passes through two Ir(α) atoms and the midpoint of two Ir(β) atoms, and the other through two Ir(β) and two S atoms. For the Ir_4 tetrahedron, only the separation between two Ir(α) atoms at 3.5353(8) Å is out of the range of the Ir−Ir bonding interaction. Among the remaining five Ir−Ir edges, the distance between two Ir(β) atoms at 2.9348(8) Å is the shortest, and the four Ir(α)−Ir(β) distances are elongated to 2.9982(7)–3.0377(7) Å. By including four Cp* ligands and two hydrido ligands, the electron count of the cluster becomes 64, which requires formally the presence of four Ir−Ir bonds

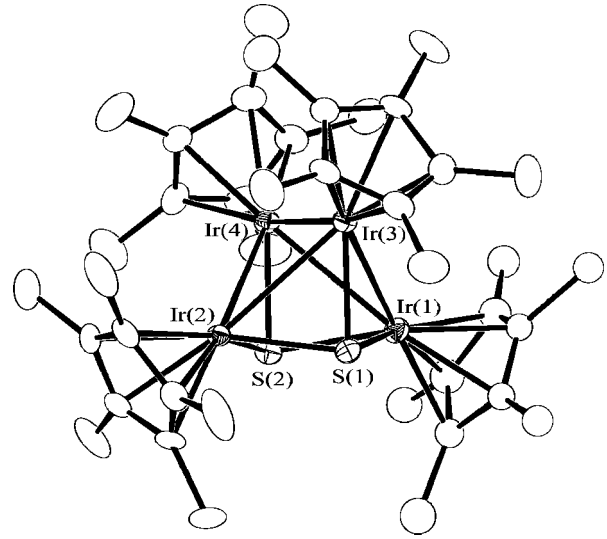

Figure 6. Molecular structure of the cationic part of **10** (thermal ellipsoids at the 30% probability level). Hydrogen atoms and the minor conformer of the disordered Cp* ligand bound to Ir(1) are omitted for clarity. Interatomic distances (Å) and bond angles (deg): Ir(1)−Ir(3), 3.0377(7); Ir(1)−Ir(4), 2.9982(7); Ir(2)−Ir(3), 3.0330(8); Ir(2)−Ir(4), 3.0131(8); Ir(3)−Ir(4), 2.9348(8); Ir(1)···Ir(2), 3.5353(8); Ir(1)−S(1), 2.337(3); Ir(1)−S(2), 2.330(4); Ir(2)−S(1), 2.336(4); Ir(2)−S(2), 2.337(3); Ir(3)−S(1), 2.290(2); Ir(4)−S(2), 2.295(2); S(1)−Ir(1)−S(2), 79.3(1); S(1)−Ir(2)−S(2), 79.2(1); Ir(1)−S(1)−Ir(2), 98.3(2); Ir(1)−S(1)−Ir(3), 82.1(1); Ir(2)−S(1)−Ir(3), 81.9(1); Ir(1)−S(2)−Ir(2), 98.5(2); Ir(1)−S(2)−Ir(4), 80.8(1); Ir(2)−S(2)−Ir(4), 81.2(1).

to satisfy the electron-precise structure. The crystal structure of **10**, having five intermetallic bonding interactions, is indicative of the delocalization of these bonds, as is suggested by the Ir−Ir distances longer than those observed in **2**–**6** (<2.9 Å). The hydrides are presumably residing at each of two Ir(α)Ir(β)$_2$ triangles, most probably as the capping ligands. The 64e cluster $[\{(\eta^6\text{-}C_6H_6)Ru\}_4(\mu_3\text{-}S)_2(\mu_3\text{-}H)_2]Cl_2$ with a closely related core structure is precedented, for which the hydrides have been located crystallographically as the μ_3-ligands.[32]

Under 1 atm of H_2, **10** was converted into **3** at 50 °C in the presence of pyridine. It should be emphasized that **10** remained intact when treated with either H_2 or pyridine alone. In the course of the reaction, the pyridinium cation formed, whose amount was almost comparable to that of **3**, as shown by the ^{1}H NMR spectra. When 100 equiv of pyridine was charged, the reaction proceeded almost cleanly without forming any cluster byproduct, yielding 95% of **3** after 16 h (eq 2). In contrast, the similar reaction using 10 equiv of pyridine occurred more slowly and reached an equilibrium mixture of **3** and **10** in a 7:3 ratio after 50 h, which is attributable to the weak acidity of pyridinium cation.

On the other hand, when *n*-butylamine was employed as an

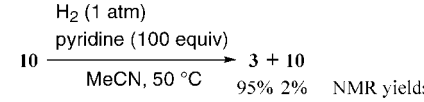

additive, reaction of **10** with H_2 provided not only **3** but also its isomer **11** as the major product (Scheme 5). For **11**, the existence of two species **11a** and **11b** equilibrating in solution was revealed from the ^{1}H NMR spectra (vide infra). The reaction

(32) Chérioux, F.; Therrien, B.; Süss-Fink, G. *Chem. Commun.* **2004**, 204.

Scheme 5

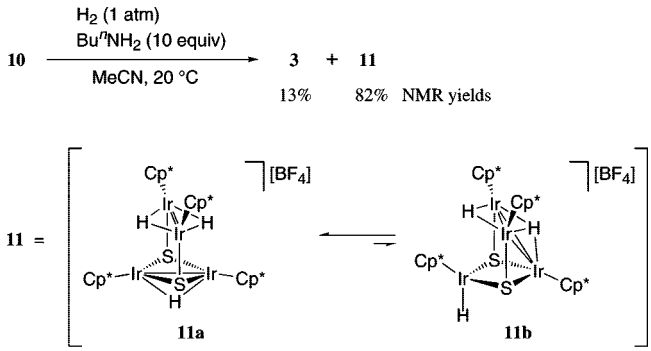

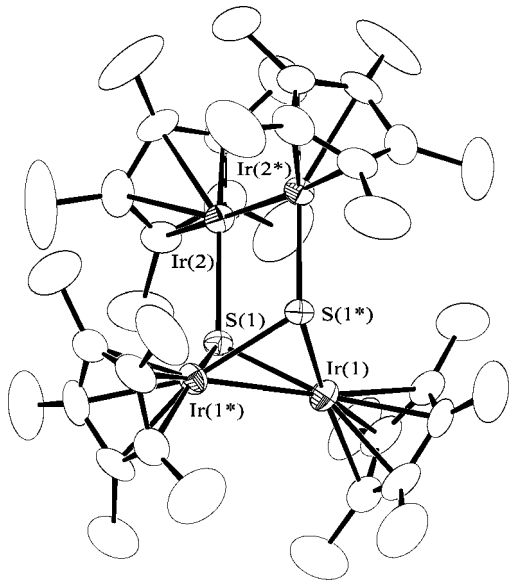

Figure 7. Molecular structure of the cationic part of **11** found in the cocrystals of **11** and **3** (90.5:9.5). Thermal ellipsoids are drawn at the 30% probability level, and hydrogen atoms are omitted for clarity. Interatomic distances (Å) and bond angles (deg): Ir(1)−Ir(1*), 2.7471(7); Ir(2)−Ir(2*), 2.7165(5); Ir(1)···Ir(2), 3.9531(8); Ir(1)···Ir(2*), 4.0076(8); Ir(1)−S(1), 2.342(3); Ir(1)−S(1*), 2.340(3); Ir(2)−S(1), 2.339(3); S(1)−Ir(1)−S(1*), 80.3(1); Ir(1)−S(1)−Ir(1*), 71.84(8); Ir(1)−S(1)−Ir(2), 115.2(1); Ir(2)−S(1)−Ir(1*), 117.8(1).

smoothly proceeded even at 20 °C under 1 atm of H_2, and **10** was completely consumed within 50 h in the presence of 10-fold molar *n*-butylamine to form **11** and **3** in 82% and 13% NMR yields, respectively. Crystallization of these products gave a mixture of **11** and **3**, whose ratio was 7:1 in bulk, and single crystals selected from this batch were applied to an X-ray crystallographic study. The crystals were found to be isomorphous to those of **3** and to contain 9–15% of **3** versus **11**. Despite the disorders mainly due to the cocrystallization with **3**, the atom-connecting scheme of **11** could be disclosed as the main component (>85%) in the crystals (Figure 7).

The cluster part of **11** belongs to the C_2 group crystallographically, but its molecular symmetry is essentially higher, C_{2v}, in contrast to the finding that the cation of **3** has only C_2 symmetry. Therefore, the structure of **11** is well interpreted on the basis of that of **10**, which is also C_{2v}. Both **10** and **11** have the same Ir−S bonding schemes, but the cluster core of **11** is elongated along the *C*2 axis in comparison with that of **10**. In **11**, short Ir−Ir distances are found between two Ir(α) atoms (Ir(1) and Ir(1*)) and between two Ir(β) atoms (Ir(2) and Ir(2*)), while the Ir(α)···Ir(β) separations larger than 3.9 Å indicate no Ir−Ir bondings between them. The major tautomer **11a** existing in solution (>90%) exhibits two 30H signals assignable to Cp* ligands in ^{1}H NMR spectrum, which correspond well to the above crystal structure of **11**. The hydrido resonances of **11a** are observed as two singlets of 1H and 2H intensities at δ −15.69 and −12.99, respectively. It might be presumed that the Ir(α)−Ir(α′) and Ir(β)−Ir(β′) edges are bridged by one and two hydrido ligands, respectively, in **11a** and solid state **11**. By taking the quality of X-ray analysis into account, the calculated bond distances in **11** should be regarded to contain some ambiguities. However, the Ir(1)−Ir(1*) and Ir(2)−Ir(2*) distances at 2.7471(7) and 2.7165(5) Å, respectively, are not exceptional in comparison with those in $[(Cp^*Ir)_2(\mu_2\text{-}SPr^i)_2(\mu_2\text{-}H)][OTf]$ at 2.7720(5) Å,[33] $[(Cp^*Ir)_2(\mu_2\text{-S-}cyclo\text{-}C_6H_{11})(\mu_2\text{-}H)_2][BPh_4]$ at 2.6085(9) Å,[34] $[(Cp^*Ir)_2(\mu_2\text{-}\eta^1,\eta^1\text{-1-pyrazolyl})(\mu_2\text{-}H)_2][BF_4]$ at 2.663(1) Å,[35] and $[(Cp^*Ir)_2(\mu_2\text{-dmpm})(\mu_2\text{-}H)_2][OTf]_2$ at 2.7236(8) Å.[25]

In contrast to the symmetric **11a**, the ^{1}H NMR resonances of **11b** reveal the existence of three kinds of Cp* ligands (1:1:2) and three inequivalent hydrido ligands, which appear at δ −16.80, −11.65, and −12.67. Small H−H coupling (J = 3.2 Hz) is observed between the former two signals. Because **11b** is the tautomer of **11a** and shows an NMR spectrum similar to that of cluster **15** (vide infra), the structure of **11b** might be characterized as that shown in Scheme 5.

On the other hand, it is expected that supplying two electrons and one proton to **10** also provides **3**; therefore, chemical reduction of **10** has been investigated. When **10** was reacted with 2 equiv of Cp_2Co in the presence of $[Et_3NH][BF_4]$ as a proton source, formation of **3** in 81% yield was confirmed by NMR measurement (eq 3). The cyclic voltammogram of **10** measured in 0.1 mol L^{-1} solution of $[Bu_4N][BF_4]$ in MeCN exhibited a irreversible reduction peak at −1.47 V vs Cp_2Fe/Cp_2Fe^+, which was slightly more negative than the Cp_2Co/Cp_2Co^+ couple at −1.35 V.[36] Nevertheless, an almost quantitative conversion of Cp_2Co into Cp_2Co^+ in the above reaction proves that two electrons have been transferred to one cluster. Presumably the protonation of **10** occurs prior to the reduction in this proton- and electron-transfer system. In fact, the reaction of **10** with Cp_2Co in MeCN without any proton source gave a complex mixture containing a small amount of **3** but no Cp_2Co^+. Although Cp^*_2Co (0/+1 at −1.91 V)[37] is strong enough to reduce **10**, reaction between them in MeCN provided not the reduced form of **10** but $[(Cp^*Ir)_3(\mu_3\text{-}S)_2]$ (**12**)[38] and a mixture of Ir-hydride species through cluster-core degradation (eq 4).

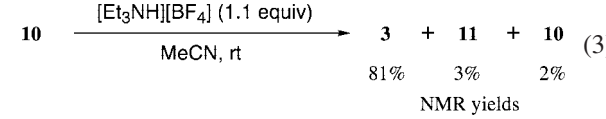

(3)

As observed for the monosulfido-capped triiridium clusters, the interconversion among the tetrairidium clusters **3**, **10**, and

(33) Iwasa, T.; Shimada, H.; Takami, A.; Matsuzaka, H.; Ishii, Y.; Hidai, M. *Inorg. Chem.* **1999**, *38*, 2851.

(34) Nishio, M.; Mizobe, Y.; Matsuzaka, H.; Hidai, M. *Inorg. Chim. Acta* **1997**, *265*, 59.

(35) Oro, L. A.; Carmona, D.; Puebla, M. P.; Lamata, M. P.; Foces-Foces, C.; Cano, F. H. *Inorg. Chim. Acta* **1986**, *112*, L11.

(36) Stojanovic, R. S.; Bond, A. M. *Anal. Chem.* **1993**, *65*, 56.

(37) Connelly, N. G.; Geiger, W. E. *Chem. Rev.* **1996**, *96*, 877.

(38) Cluster **12** has been previouly prepared by reduction of **8**, although its solid-state structure has not been revealed yet.[20] We have crystallographically determined **12**, and the result is added in the Supporting Information.

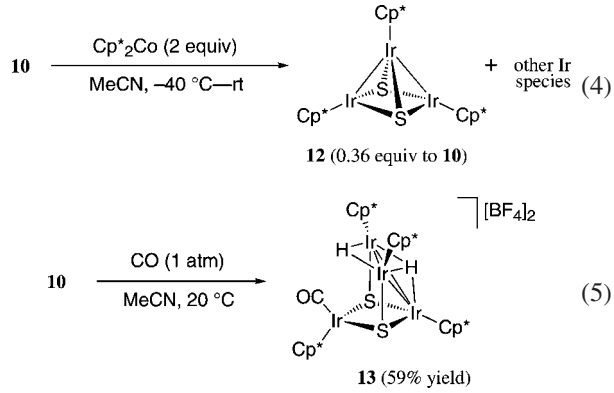

11 proceeds with retention of all Ir−S bonds in spite of the changes in the coordination mode of the hydrido ligands. If the reaction converting **10** to **3** by a protonation and two-elecron reduction (eq 3) is coupled with that regenerating **10** from **3** by a protonation and subsequent liberation of H_2 (eq 1), it turns out that production of H_2 gas from two protons and two electrons is accomplished. Interestingly, cluster **10** not only mediates this H_2 production but also proves effective to the heterolytic cleavage of H_2 into a hydride and a proton.[39] To elucidate the interaction mechanisms between **10** and H_2, further coordination chemistry of **10** has been investigated as described below.

Reactivities of 10 toward *σ*-Donor Ligands. When an MeCN solution of **10** was stirred under CO atmosphere at room temperature, one CO molecule was incorporated to form the cluster $[(Cp^*Ir)_4(\mu_3\text{-}S)_2(\mu\text{-}H)_2(CO)][BF_4]_2$ (**13**) (eq 5). The molecular structure of **13** has been determined unambiguously by X-ray analysis, and Figure 8 shows the structure of one of two crystallographically independent but essentially identical cluster cations. The CO ligand coordinates to one of two Ir(α) atoms (Ir(1)) in an end-on fashion and oriented in the direction syn to the Ir(*β*) atoms (Ir(3) and Ir(4)) with respect to the Ir(1)Ir(2)S_2 ring (endo form). As a result, the Ir(1) atom is separated from two Ir(*β*) centers further by ∼0.9 Å, canceling the bonding interactions. Three Ir−Ir bonds inside the Ir(2)Ir(*β*)$_2$ triangle are retained, being decreased to 2.8523(6)–2.8863(7) Å in comparison with those in **10**. The ^{1}H NMR spectrum of **13** exhibits three Cp* signals with an intensity ratio of 1:1:2 assignable to two inequivalent Ir(α) and two equivalent Ir(*β*) sites. Two hydrido ligands are observed as two separated signals at δ −16.75 and −10.95 mutually coupling with 4.4 Hz, which are assumed to be at the Ir(*β*)$_2$ edge and at the Ir(2)Ir(*β*)$_2$ face. The bonding parameters of the CO ligands as well as its IR absorption at 1992 cm^{-1} are typical of the terminal ones,[40] indicating the absence of semibridging or other secondary interactions.

In contrast to the exclusive formation of **13** from **10** and CO, addition of 1 equiv of XyNC to **10** smoothly proceeded at 0 °C to give two kinds of adducts (∼5:2 in the crude mixture). Standing the solution at higher temperatures or addition of an excess amount of XyNC led to slow decomposition of the products, yielding **8** and uncharacterized complexes. Crystallization of the products at −20 °C afforded dark red prisms and red platelets, X-ray diffraction study of which clearly disclosed their structures as endo (**14**) and exo (**15**) isomers of $[(Cp^*Ir)_4(\mu_3\text{-}S)_2(\mu\text{-}H)_2(CNXy)][BF_4]_2$, respectively (eq 6). Each

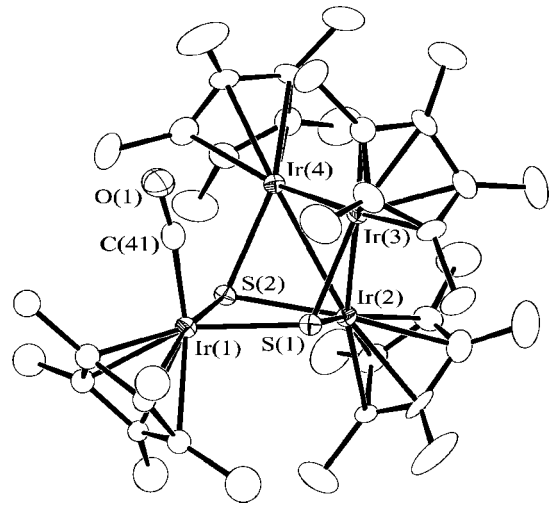

Figure 8. One of two independent cations in the crystal structure of **13** (thermal ellipsoids at the 30% probability level). Hydrogen atoms and the minor conformer of the disordered Cp* ligand bound to Ir(1) are omitted for clarity. Interatomic distances (Å) and bond angles (deg) with the corresponding values in the second cation, where Ir(*β*) denotes Ir(3) or Ir(4): Ir(2)−Ir(*β*), 2.8761(7)–2.8863(7); Ir(3)−Ir(4), 2.8523(6), 2.8561(6); Ir(1)···Ir(2), 3.6961(6), 3.6957(6); Ir(1)···Ir(*β*), 3.9233(6)–3.9285(6); Ir(1)−S, 2.375(3)–2.392(3); Ir(2)−S, 2.343(3)–2.356(3); Ir(*β*)−S, 2.311(3)–2.322(3); Ir(1)−C(41), 1.85(2), 1.87(2); O(1)−C(41), 1.15(2), 1.16(2); S−Ir(1)−S, 75.6(1), 75.6(1); S−Ir(1)−C(41), 94.8(7)–95.2(4); S−Ir(2)−S, 77.0(1), 76.9(1);Ir(1)−S−Ir(2),102.2(1)–103.1(1);Ir(1)−S−Ir(*β*),112.9(1)–113.7(1); Ir(2)−S−Ir(*β*), 75.9(1)–76.7(1); Ir(1)−C(41)−O(1), 171(1), 171(1).

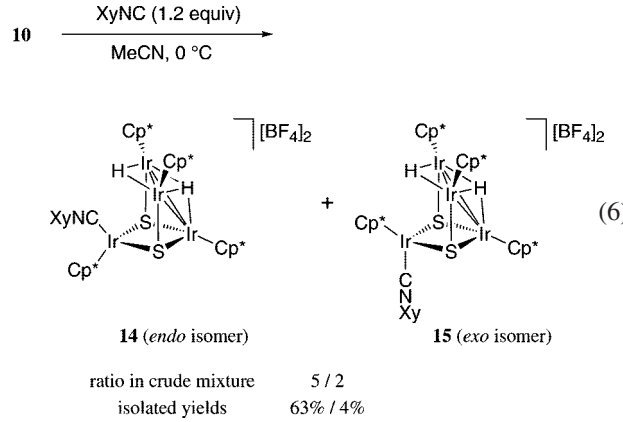

isomer exhibits a ^{1}H NMR spectral pattern analogous to **13** except for those of the XyNC ligand, and isomerization between the major **14** and the minor **15** does not occur in solution at room temperature. The molecular structure of **14** depicted in Figure 9 is analogous to that of **13**, where XyNC coordinates to the Ir(1) atom instead of CO. The bonding parameters of the cluster cores of **13** and **14** are essentially identical, although the Ir(1)···Ir(*β*) distances in **14** are slightly elongated, owing to incorporation of a larger XyNC molecule. The Ir_4S_2 framework in **15** is also the same as those of **13** and **14**, but only the stereochemistry around the Ir(1) center differs in **15**, as shown in Figure 10. Thus, the coordinated XyNC resides at the side anti to the Ir(*β*) atoms with respect to the Ir(α)$_2S_2$ ring. Between **14** and **15**, remarkable differences in bond lengths and angles are not found in the Ir-CNXy moieties, while the IR absorptions for the C≡N stretching mode are observed at 2089 and 2118 cm^{-1}, respectively. Concomitant producion of the exo-isomer **15** in the reaction with XyNC is probably because the endo-

(39) (a) Kubas, G. J. *Adv. Inorg. Chem.* **2004**, *56*, 127. (b) Morris, R. H. *Can. J. Chem.* **1996**, *74*, 1907. (c) Brothers, P. *Prog. Inorg. Chem.* **1981**, *28*, 1.

(40) The C≡O stretching frequencies of the related complexes are 1974–2021 cm^{-1}.[11]

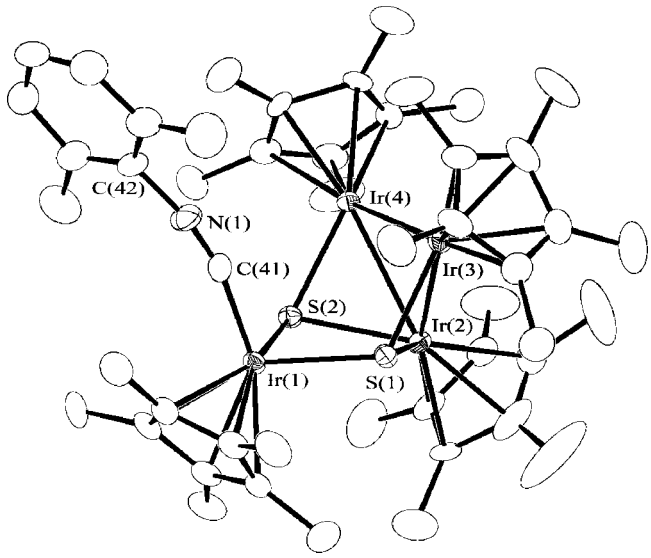

Figure 9. Molecular structure of the cationic part of **14** (thermal ellipsoids at the 30% probability level). Hydrogen atoms are omitted for clarity. Interatomic distances (Å) and bond angles (deg): Ir(2)−Ir(3), 2.8954(5); Ir(2)−Ir(4), 2.8572(4); Ir(3)−Ir(4), 2.8461(6); Ir(1)···Ir(2), 3.6696(6); Ir(1)···Ir(3), 3.9900(5); Ir(1)···Ir(4), 4.0009(6); Ir(1)−S(1), 2.366(3); Ir(1)−S(2), 2.397(3); Ir(1)−C(41), 1.92(1); Ir(2)−S(1), 2.348(3); Ir(2)−S(2), 2.360(2); Ir(3)−S(1), 2.296(3); Ir(4)−S(2), 2.338(3); N(1)−C(41), 1.16(1); N(1)−C(42), 1.40(1); S(1)−Ir(1)−S(2), 76.03(9); S(1)−Ir(1)−C(41), 104.8(4); S(2)−Ir(1)−C(41), 91.9(4); S(1)−Ir(2)−S(2), 77.08(9); Ir(1)−S(1)−Ir(2), 102.23(9); Ir(1)−S(1)−Ir(3), 117.70(9); Ir(2)−S(1)−Ir(3), 77.1(1); Ir(1)−S(2)−Ir(2), 100.94(8); Ir(1)−S(2)−Ir(4), 115.3(1); Ir(2)−S(2)−Ir(4), 74.92(8); Ir(1)−C(41)−N(1), 166(1); C(41)−N(1)−C(42), 167(1).

coordination of sterically large XyNC is less advantageous than that of CO. In addition, higher C≡N stretching frequency of **15** than that of **14** may suggest the weaker π-back-donating ability to XyNC in the exo-form, and for the coordination of the strong π-acceptor such as CO the exo-form is disfavored.

It was also found that **10** slowly reacted with excess N_2H_4 in

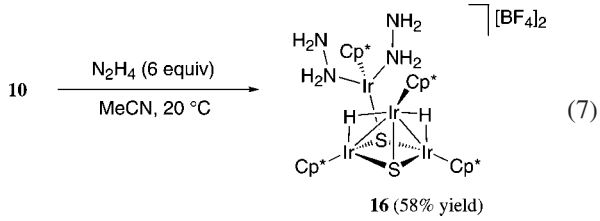

16 (58% yield) (7)

MeCN solution at room temperature to afford the 1:2 adduct $[(Cp^*Ir)_4(\mu_3\text{-}S)_2(\mu_2\text{-}H)_2(N_2H_4)_2][BF_4]_2$ (**16**) (eq 7). Surprisingly, this reaction is quite specific for N_2H_4, and neither substituted hydrazines nor other N-donors listed in Table 1 (vide infra) react with **10**.[41] Coordination of N_2H_4 in **16** is not so strong that partial regeneration of **10** by releasing N_2H_4 occurs in solution at ambient temperature. X-ray crystallography revealed the structure of the dication of **16** as presented in Figure 11. The most remarkable feature is that one of the Ir(β) sites, Ir(3), binds two N_2H_4 each in an η^1-fashion. The Ir(3) fragment is connected to the Ir_3 cluster scaffold only by an Ir−S bond and adopts a three-legged piano-stool geometry with 18-electron configuration. The Ir−N bond lengths at 2.16(2) and 2.15(2) Å are normal in comparison with other hydrazine complexes.[42,43] Separations between the Ir(4) atom and each of two Ir(α) centers at 2.907(1) and 2.940(1) Å suggest that each Ir(4)−Ir(α) edge is presumed to possess a μ_2-hydrido ligand. The Ir−S(1) bonds are elongated by ∼0.1 Å or more in comparison with the Ir−S(2) bond. The ^{1}H NMR spectrum of **16** consistently shows three Cp* signals in a 1:1:2 ratio together with one singlet assignable to two hydrido ligands. The noncoordinated NH_2 protons of hydrazine ligands are slightly shifted to lower field at δ 3.80 in comparison with free N_2H_4 (δ 2.94), while the inner NH_2 protons are diastereotopically observed at δ 5.63 and 6.29. In addition, the IR spectrum exhibits the ν(N−H) bands in the region of 3260–3390 cm^{-1}. Although we cannot rationally explain the reason why only N_2H_4 adds to **10** among many N-donors, the adduct may be stabilized by intramolecular hydrogen bonds between two coordinated N_2H_4 inside the bowl-like space. The existence of the intramolecular N−H···N bonds in *cis*,*trans*-$[IrH_2(PCy_3)_2(N_2H_4)_2]^+$ (Cy = *cyclo*-C_6H_{11}) has been claimed.[44]

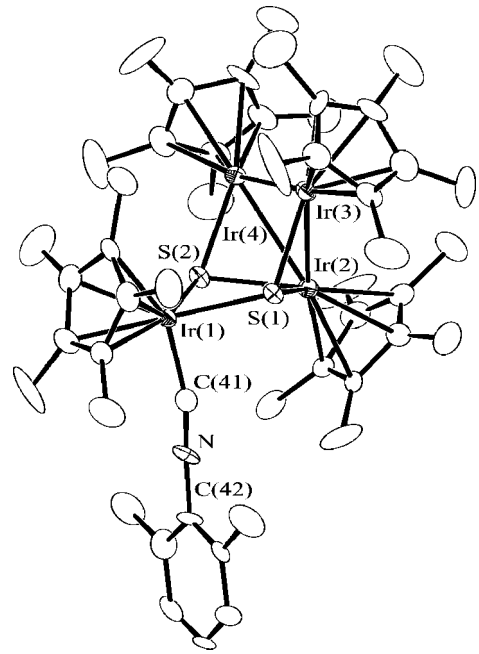

Figure 10. Molecular structure of the cationic part of **15** (thermal ellipsoids at the 30% probability level). Hydrogen atoms are omitted for clarity. Interatomic distances (Å) and bond angles (deg): Ir(2)−Ir(3), 2.8965(7); Ir(2)−Ir(4), 2.9102(7); Ir(3)−Ir(4), 2.8235(7); Ir(1)···Ir(2), 3.6228(6); Ir(1)···Ir(3), 4.0550(7); Ir(1)···Ir(4), 4.0580(7); Ir(1)−S(1), 2.385(3); Ir(1)−S(2), 2.393(3); Ir(1)−C(41), 1.91(1); Ir(2)−S(1), 2.362(3); Ir(2)−S(2), 2.363(3); Ir(3)−S(1), 2.330(3); Ir(4)−S(2), 2.317(4); N−C(41), 1.20(2); N−C(42), 1.38(2); S(1)−Ir(1)−S(2); 77.0(2); S(1)−Ir(1)−C(41), 91.8(4); S(2)−Ir(1)−C(41), 90.7(4); S(1)−Ir(2)−S(2), 78.1(1); Ir(1)−S(1)−Ir(2), 99.5(1); Ir(1)−S(1)−Ir(3), 118.6(2); Ir(2)−S(1)−Ir(3), 76.3(1); Ir(1)−S(2)−Ir(2), 99.2(1); Ir(1)−S(2)−Ir(4), 119.0(2); Ir(2)−S(2)−Ir(4), 76.9(1); Ir(1)−C(41)−N, 166(1); C(41)−N−C(42), 171(2).

In summary of this section, it has been proved that **10** readily opens the coordination sites by cleavage of the Ir−μ-H bonds. On the contrary, all Ir−S bonds are retained during the coordination of any σ-donors, which prevents the Ir_4 assembly

(41) Formation of only the analogous NH_3 adduct $[(Cp^*Ir)_4(\mu_3\text{-}S)_2(\mu_2\text{-}H)_2(NH_3)_2][BF_4]_2$ was confirmed spectoscopically, but 55% of unreacted **10** remained after 110 h at room temperature even when 10-fold molar excess of NH_3 was added. ^{1}H NMR (CD_3CN): δ −18.14 (s, 2H, hydride), 1.63, 2.23 (s, 15H each, Cp*), 1.83 (s, 30H, Cp*).

(42) Bergs, R.; Sünkel, K.; Robl, C.; Beck, W. *J. Organomet. Chem.* **1997**, *533*, 247.
(43) Hoffmüller, W.; Polborn, K.; Krossing, I.; Nöth, H.; Beck, W. *J. Organomet. Chem.* **1999**, *577*, 93.
(44) Xu, W.; Lough, A. J.; Morris, R. H. *Inorg. Chem.* **1996**, *35*, 1549.

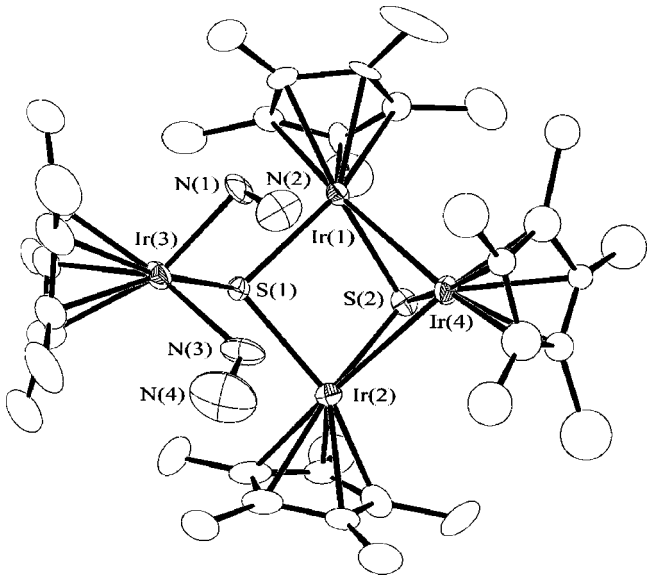

Figure 11. Molecular structure of the cationic part of **16** (thermal ellipsoids at the 30% probability level). Hydrogen atoms and the minor conformer of the disordered Cp* ligand bound to Ir(4) are omitted for clarity. Interatomic distances (Å) and bond angles (deg): Ir(1)−Ir(4), 2.907(1); Ir(2)−Ir(4), 2.940(1); Ir(1)···Ir(2), 3.527(1); Ir(1)···Ir(3), 4.204(1); Ir(2)···Ir(3), 4.181(1); Ir(1)−S(1), 2.419(5); Ir(1)−S(2), 2.320(6); Ir(2)−S(1), 2.413(5); Ir(2)−S(2), 2.319(5); Ir(3)−S(1), 2.450(5); Ir(3)−N(1), 2.16(2); Ir(3)−N(3), 2.15(2); Ir(4)−S(2), 2.308(6); N(1)−N(2), 1.46(3); N(3)−N(4), 1.38(4); S(1)−Ir(1)−S(2), 81.0(2); S(1)−Ir(2)−S(2), 81.2(2); S(1)−Ir(3)−N(1), 87.9(6); S(1)−Ir(3)−N(3), 83.5(6); N(1)−Ir(3)−N(3), 82.8(8); Ir(1)−S(1)−Ir(2), 93.8(2); Ir(1)−S(1)−Ir(3), 119.4(2); Ir(2)−S(1)−Ir(3), 118.6(2); Ir(1)−S(2)−Ir(2), 99.0(2); Ir(1)−S(2)−Ir(4), 77.8(2); Ir(2)−S(2)−Ir(4), 78.9(2); Ir(3)−N(1)−N(2), 112(1); Ir(3)−N(3)−N(4), 120(2).

from degrading. The nature of the donor molecule probably determines the site to bind among the two distinct centers, Ir(α) and Ir(*β*). From the number of coordinated sulfido ligands, the former center is estimated to be more *π*-donating than the latter. Thus, *π*-acceptor ligands such as CO and XyNC bind to Ir(α) exclusively. Coordination of hydrazine to the Ir(*β*) suggests the potential availability of this center for binding certain good *σ*-donor ligands, which provides two coordination sites by removing two Ir−*μ*-H bonds.

Mechanisms Proposed for the Hydrido Incorporation to 10. Taking the above findings into consideration, the mechanism for the reactions of **10** with H_2 in the presence of base is discussed here. To clarify the origin of hydrido ligands in the products **3** and **11**, these reactions were carried out by using D_2. When **10** was treated with D_2 and pyridine as shown in eq 8, the reaction mixture contained monodeuterated **3** and nondeuterated **10** after 25 h.[45] The hydrido region of the ^{1}H NMR spectrum depicted in Figure 12 clearly indicates the presence of two **3**-d_1 species, for which the deuterated positions differ from each other. The ratio of these symmetric (*sym*) and asymmetric (*asym*) isomers of **3**-d_1 coincides with the statistic distribution of 1:2. The absence of either nondeuterated or multiply deuterated **3** is also confirmed from the shape and integration of the hydrido signals. When the reaction of **10** with *n*-butylamine was conducted under D_2, one deuterido ligand was selectively incorporated into the Ir(α)$_2$ edge of **11a**, and deuteration of the hydrido bridges at the Ir(*β*)$_2$ site was not

(45) The reverse reaction was negligible at that period, since attaining equilibrium of **3** and **10** took a much longer time (> 50 h).

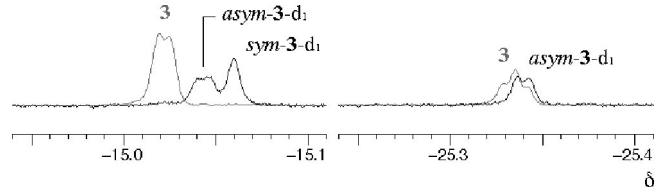

Figure 12. ^{1}H NMR spectrum (hydrido region) of the mixture of *sym*- and *asym*-**3**-d_1 obtained after 25 h under conditions indicated in eq 8. The spectrum of nondeuterated **3** is overlaid in gray lines, and intensities of both spectra are normalized based on the Cp* signals.

observed at all (eq 9). Similarly, only the signal of the terminal hydride (*δ* −12.67) disappeared in the ^{1}H NMR spectrum of **11b**, and *sym*- and *asym*-**3**-d_1 were concurrently formed in a 1:2 ratio.

The reactions of **10** with H_2 were also promoted by other

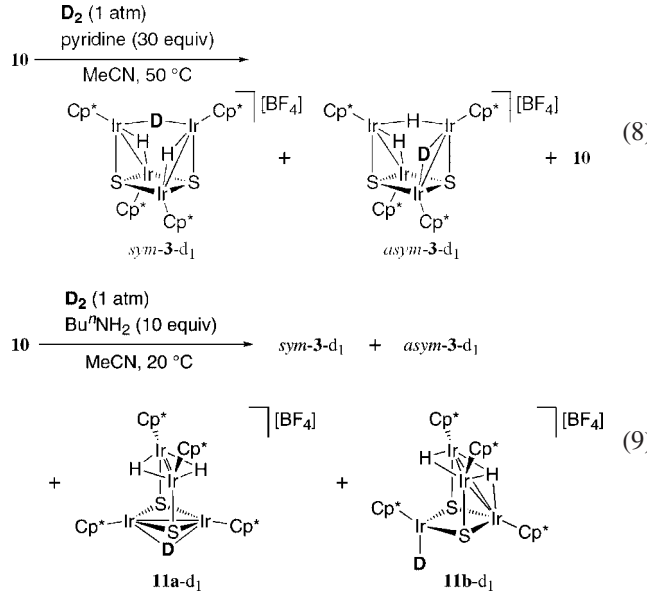

aliphatic amines. Although the reaction rates and the **3**/**11** ratios considerably varied, all the reactions with aliphatic amines proceeded until **10** was completely converted, and the **3**/**11** ratio was almost constant during the course of the reactions. The effects of various organonitrogen additives were compared under the same conditions as shown in Table 1, in which representative data were collected. There is a tendency that conversion rates are not influenced by the basicity of amines but remarkably retarded by the steric hindrance around nitrogen atom. It is also found that sterically emcumbered amines generally lower the selectivities of **11**. Reactions with bases much weaker than alkylamines (pK_b = 3–4), such as pyridine and aniline (pK_b = 8.64 and 9.38, respectively), are slower and do not afford **11**.

Incorporation of the hydrido ligand into **10** undoubtedly proceeds via formation of the intermediary adduct of **10** and H_2 followed by deprotonation.[46] The experiments using D_2 demonstrate that one D atom of a D_2 molecule and both of two hydrido ligands of **10** are contained in **3** or **11**, indicating that proton abstraction occurs strictly for the H atoms originated

(46) The reaction that proceeds in a sequence different from this proposal has been known. Thus, $[\{Cp^*Ir(CO)\}_2(\mu\text{-}H)_2]^{2+}$ is deprotonated by base to afford $[\{Cp^*Ir(CO)\}_2(\mu\text{-}H)]^+$, which then reacts with H_2 to form $[\{Cp^*IrH(CO)\}_2(\mu\text{-}H)]^+$. Heinekey, D. M.; Fine, D. A.; Barnhart, D. *Organometallics* **1997**, *16*, 2530.

Table 1. Reactions of 10 with Organic Bases under H_2 Atmosphere[a]

base	time (h)	ratio of clusters[b] (**3**:**11**:**10**)
pyridine	50	41:0:59
$PhNH_2$	25	6:0:94
Et_3N	75	48:24:28
Et_2NH	75	51:33:16
pyrrolidine	25	19:73:8
Bu^nNH_2	25	8:85:7
$EtMe_2CNH_2$	75	58:21:21
$H_2N(CH_2)_2NH_2$	25	15:85:0

[a] Conditions: **10** (0.010 mmol), base (0.030 mmol), MeCN (3 mL), H_2 (1 atm), 50 °C. [b] Determined by ^1H NMR.

from the H_2 molecule before it exchanges with the hydrido ligands. It is also certain that hydrido ligands in **10** as well as **3** and **11** do not exchange with D_2 under these conditions. Because coordination of some donor molecules to **10** occurs at a single Ir center without any direct interaction with hydrido ligands, the first interaction with H_2 is also presumed to take place at only one Ir atom. This postulation is supported by the fact that heterolytic cleavage of a H_2 molecule on the Ir(III) centers has ubiquitously been found.[47] Some of such reactions have been disclosed to proceed definitely by deprotonation of η^2-H_2 complexes.[48]

Although the H_2 adducts of **10** have not been detectable, several modes of interaction can be proposed as illustrated in Scheme 6. Binding of H_2 to the Ir(α) atom from the exo direction forms **A**, whose deprotonation is the most probable pathway to **11**, as suggested by selective incorporation of the deuterido ligand on the Ir(α)$_2$ edge. On the other hand, several intermediates leading to **3** can be assumed such as **B** or **C** (and its derivative **C′**), in which H_2 is bound to the Ir(α) center in an endo form or rather to the Ir(*β*) center, respectively. Statistic distribution of D in **3**-d_1 is probably the consequence of intramolecular site exchange between hydrido ligands in **3** and is not likely, indicating the reaction pathway. Whether the H_2 molecule is only attached as a dihydrogen ligand or it is cleaved to dihydride, the Ir(*β*) center is estimated to be able to activate the hydrogen atom to a more strongly acidic one than the Ir(α) due to the difference in electron density at the metal. Therefore, the acidity of **A** may be too weak to be deprotonated by pyridine. Although basicities of alkylamines are strong enough to deprotonate **A**, bulky amines are not so reactive probably due to the steric barrier of Cp* ligands at the Ir(α) sites. In this regard, deprotonation of **B** is certainly much more retarded by steric effects, so it is likely that formation of **3** proceeds via **C** or less hindered **C′**, where the structure of the latter is closely related to **16**. The fact that **A** becomes the major pathway in the reactions with small alkylamines may be rationalized by more facile formation of **A** than **C** or **C′**.

Scheme 6

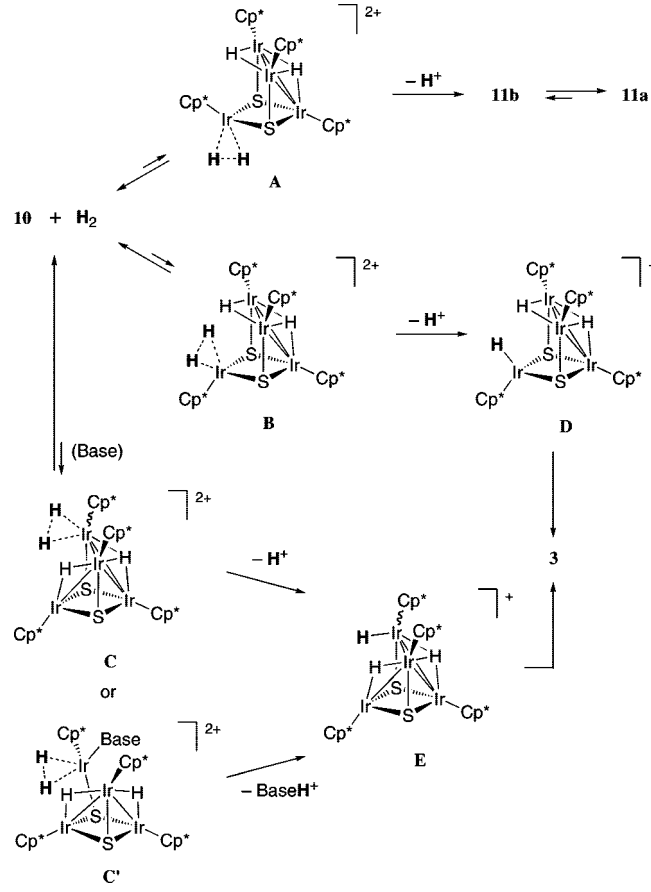

Conclusion

In this work, we have shown different characteristics of the hydrido ligands in the various sulfido clusters consisting of only Ir(III) centers. The hydrido ligand in tetranuclear cluster **3** appears to be *hydridic* from the reactivity in evolving H_2 by protonation. In contrast, the hydrido ligand in trinuclear **2** is *protic* and can be abstracted by base instead of undergoing protonation to release H_2. In fact, **2** can be prepared by protonation of **7**, whose hydrido ligands do not undergo protonation to form H_2. Reversible deprotonation of the *μ*-hydrido ligands in the cationic Ir(III)$_2$ complexes has been demonstrated previously for $[(Cp^*Ir)_2(\mu\text{-}SPr^i)_2(\mu\text{-}H)]^+$ and **1**.[33,49,50] With respect to the cluster composition, **3** is built up by adding a neutral Cp*IrS unit to **2**, which is recognized further to consist of **1** and a Cp*IrS. This implies that reactivities of the hydrido ligands are related to the number of the core Ir and S atoms. Expansion of the cluster core increases intermetallic d-orbital overlappings which probably stabilize the state of fewer cluster-electrons. Thus, loss of H_2 is readily compensated by Ir−Ir bond formation. It is noteworthy that previous reports on the mononuclear complexes $[Cp^{\#}IrH_2(L)]$ ($Cp^{\#}$ = Cp or pentaalkylated Cp; L = CO, phosphines, phosphites) have revealed, by contrast, that protonation affords the Ir(V) complex $[Cp^{\#}IrH_3(L)]^+$ at first, hydrogen loss from which is accelerated as the electron density at the metal decreased.[30a,51,52]

(47) (a) White, C.; Oliver, A. J.; Maitlis, P. M. *J. Chem. Soc., Dalton Trans.* **1973**, 1901. (b) Gill, D. S.; Maitlis, P. M. *J. Organomet. Chem.* **1975**, *87*, 359. (c) Maitlis, P. M. *Acc. Chem. Res.* **1978**, *11*, 301. (d) Ogo, S.; Nakai, H.; Watanabe, Y. *J. Am. Chem. Soc.* **2002**, *124*, 597.

(48) (a) Crabtree, R. H. *Acc. Chem. Res.* **1990**, *23*, 95. (b) Esteruelas, M. A.; Herrero, J.; López, A. M.; Oro, L. A.; Schulz, M.; Werner, H. *Inorg. Chem.* **1992**, *31*, 4013. (c) Albinati, A.; Bakhmutov, V. I.; Caulton, K. G.; Clot, E.; Eckert, J.; Eisenstein, O.; Gusev, D. G.; Grushin, V. V.; Hauger, B. E.; Klooster, W. T.; Koetzle, T. F.; McMullan, R. K.; O'Loughlin, T. J.; Pélissier, M.; Ricci, J. S.; Sigalas, M. P.; Vymenits, A. B. *J. Am. Chem. Soc.* **1993**, *115*, 7300. (d) Bianchini, C.; Moneti, S.; Peruzzini, M.; Vizza, F. *Inorg. Chem.* **1997**, *36*, 5818. (e) Gruet, K.; Clot, E.; Eisenstein, O.; Lee, D. H.; Patel, B.; Macchioni, A.; Crabtree, R. H. *New J. Chem.* **2003**, *27*, 80.

(49) Nishio, M.; Matsuzaka, H.; Mizobe, Y.; Hidai, M. *Inorg. Chim. Acta* **1997**, *263*, 119.

(50) Hou, Z.; Koizumi, T.; Fujita, A.; Yamazaki, H.; Wakatsuki, Y. *J. Am. Chem. Soc.* **2001**, *123*, 5812.

(51) Heinekey, D. M.; Millar, J. M.; Koetzle, T. F.; Payne, N. G.; Ziilm, K. W. *J. Am. Chem. Soc.* **1990**, *112*, 909.

On the other hand, modeling the function of hydrogenase is receiving much attention from its potential in the new and efficient H_2 production process. Active sites of metalloenzymes that accomplish proton reduction or other electron-transfer reactions often consist of sulfur-bridged polymetallic chromophores. Electrochemical reduction of protons has been investigated intensively by using thiolate-bridged diiron complexes, while some studies on clusters of larger cores such as Fe_4S_4 have also appeared.[53] In this work, we have found stepwise reduction of protons into H_2 on the tetrairidium cluster **10**. Electrochemical reactions mediated by large clusters like this are of much interest because larger cluster cores are expected to have an advantage in multiple electron transfer over smaller ones. For instance, more than six electrons are required in biological reduction of N_2 to NH_3, which is catalyzed by nitrogenase having the active site of a $MoFe_7S_9$ core. Electrocatalytic proton reduction using **10** as well as electron transfer to the small molecules coordinated to **10** are now under investigation.

Experimental Section

General Considerations. All manipulations were performed under nitrogen atmosphere using standard Schlenk techniques. Solvents were dried by common procedures and distilled under nitrogen before use. Complex **1** was prepared according to a literature method.[47a] Other reagents were commercially available and used as received. Yields were calculated on the basis of the iridium atom except for those stated otherwise.

^{1}H NMR spectra (400 MHz) were recorded on a JEOL alpha-400 spectrometer, and chemical shifts were referenced using those of residual solvent resonances ($CDCl_3$ at 7.26, C_6D_6 at 7.15, and CD_3CN at 1.93). Line-shape analysis of the VT ^{1}H NMR spectra was carried out with the gNMR program package.[54] IR and mass spectra were recorded on JASCO FT/IR-420 and JEOL JMS600H spectrometers. Elemental analyses were done with a Perkin-Elmer 2400 series II CHN analyzer. Quantitative analyses of H_2 in the gas phase were performed on a Shimadzu GC-14B gas chromatograph equipped with a molecular sieve 13X column. Cyclic voltammograms were measured on a BAS CV-50W electrochemical analyzer using a glassy carbon working electrode with a scan rate of 100 mV s^{-1}.

Reaction of 1 with NaSH (Ir/S = 3:2). A MeOH (3 mL) solution of NaSH (21 mg, 0.38 mmol) was added dropwise to a solution of **1** (426 mg, 0.571 mmol) in MeOH (15 mL) at room temperature over a period of 5 h. After the mixture was stirred for a further 15 h, the deposited dark red solid was filtered off and recrystallized from toluene (1 mL)/MeOH (10 mL) at −20 °C to give dark red prisms of $[(Cp^*IrH)_2(Cp^*Ir)(\mu_3\text{-}S)(\mu_2\text{-}H)_2]$ (**4**; 4 mg, 0.9% yield) and orange prisms of $[(Cp^*IrH)_4(\mu_4\text{-}S)(\mu_2\text{-}H)_2]$ (**5**; 2 mg, 0.5% yield). The above dark brown filtrate containing **2** and **3** in a ∼5:3 molar ratio was evaporated to dryness, and the residue was washed repeatedly with benzene (∼15 mL) and then extracted with THF (45 mL). The remaining solid was dissolved in CH_2Cl_2 (3 mL), and addition of hexane (50 mL) to the filtered CH_2Cl_2 solution afforded reddish-brown prisms of $[(Cp^*Ir)_4(\mu_3\text{-}S)_2(\mu_2\text{-}H)_3][BF_4]$ (**3**, 71 mg, 17% yield). The above THF extract was dried, and the residue was crystallized from MeCN (1 mL)/ether (18 mL) to give red plates of $[(Cp^*Ir)_3(\mu_3\text{-}S)(\mu_2\text{-}H)_3][BF_4]\cdot 0.5(Et_2O)$ (**2**·0.5(Et_2O), 139 mg, 32% yield). **2**·0.5(Et_2O): ^{1}H NMR ($CDCl_3$): δ −21.86 (s, 3H, hydride), 2.24 (s, 45H, Cp*), 1.11 (t, 3H, CH_3 of Et_2O), 3.41 (q, 2H, CH_2 of Et_2O). FAB MS (*m*-nitrobenzyl alcohol): 1017 (cation with correct isotopic pattern). Anal. Calcd for $C_{32}H_{53}O_{0.5}BF_4SIr_3$: C, 33.68; H, 4.68. Found: C, 33.30; H, 4.74. **3**: ^{1}H NMR ($CDCl_3$): δ −25.34 (br t, 1H, $J \sim 2$ Hz, hydride), −15.02 (br d, 2H, $J \sim 2$ Hz, hydride), 1.97, 2.03 (s, 30H each, Cp*). FAB MS (*m*-nitrobenzyl alcohol): 1377 (cation with correct isotopic pattern). Anal. Calcd for $C_{40}H_{63}BF_4S_2Ir_4$: C, 32.82; H, 4.34. Found: C, 32.73; H, 4.22. **4**: ^{1}H NMR (THF-d_8, −20 °C): δ −19.90, −19.84, −17.47, −15.53 (br s, 1H each, hydride), 1.91, 2.00, 2.09 (s, 15H each, Cp*). ^{1}H NMR (THF-d_8, 55 °C): δ −19.91 (vbr, 2H, hydride), −17.57, −15.64 (vbr, 1H each, hydride), 1.97 (vbr, 30H, Cp*), 2.10 (s, 15H, Cp*). IR (KBr): ν(Ir−H) 2148, 2104 cm^{-1}. Anal. Calcd for $C_{30}H_{49}SIr_3$: C, 35.38; H, 4.85. Found: C, 35.37; H, 4.93. **5**: ^{1}H NMR (C_6D_6): δ −19.06 (br t, 2H, $J \sim 3$ Hz, bridging hydride), −17.37 (br d, 4H, $J \sim 3$ Hz, terminal hydride), 1.97 (s, 60H, Cp*). IR (KBr): ν(Ir−H) 2080 cm^{-1}. Anal. Calcd for $C_{40}H_{66}SIr_4$: C, 35.64; H, 4.94. Found: C, 35.64; H, 5.03.

Reaction of 1 with NaSH (Ir/S = 1:1). To a MeOH solution (40 mL) of **1** (1.125 g, 1.51 mmol) was added a MeOH solution of NaSH (85 mg, 1.5 mmol) dropwise over 5 h at room temperature. After stirring the mixture for a further 15 h, a dark red solid was filtered off and recrystallized from toluene (2 mL)/MeOH (15 mL) at −20 °C to afford crystals of **4** (40 mg, 4% yield) and **5** (7 mg, 0.7% yield). The above MeOH filtrate was evaporated under vacuum, and the residue was extracted with benzene (20 mL). From the remaining solid, crystals of **2**·0.5(Et_2O) (30 mg, 3% yield) were obtained by extraction with THF (35 mL) followed by crystallization from MeCN (1 mL)/ether (18 mL), and **3** (196 mg, 18% yield) was isolated by further extraction with CH_2Cl_2 (5 mL) and slow diffusion of hexane (15 mL) to this extract.

The former benzene extract was dried, and MeOH (8 mL) was added to the residue. A small amount of black solid was filtered off and recrystallized repeatedly from toluene/MeOH at −20 °C to provide dark green crystals of $[(Cp^*Ir)_5Ir(\mu_3\text{-}S)_5H]\cdot 0.5(\text{toluene})$ (**6**·0.5(toluene), 10 mg, 1.5% yield). To the MeOH filtrate containing $[(Cp^*Ir)_3(\mu_3\text{-}S)H_2]$ (**7**) as the major product was added $[Et_2OH][BF_4]$ (140 μL, 1.02 mmol), and the mixture was stirred at room temperature for 18 h. The volatiles of the resulting solution were evaporated under vacuum, and the residual oily material was washed repeatedly with benzene (20 mL) and then extracted with $CHCl_3$ (20 mL). The residual dark brown oil was crystallized from MeCN (4 mL)/ether (16 mL) to give a mixture (total 40 mg) of yellow crystals of $[(Cp^*Ir)_3(\mu_3\text{-}S)_2][BF_4]_2$ (**8**) and dark brown plates of $[(Cp^*Ir)_4Ir(\mu_3\text{-}S)_4][BF_4]_3$ (**9**). Crystallization of the above $CHCl_3$ extract from MeCN (1 mL)/ether (18 mL) afforded crystals of **2**·0.5(Et_2O) (429 mg, 37% yield). **6**·0.5(toluene): ^{1}H NMR (C_6D_6): δ −13.31 (s, 1H, hydride), 1.75, 1.92, 2.74 (s, 15H each, Cp*), 2.10 (s, 30H, Cp*). Anal. Calcd for $C_{53.5}H_{80}S_5Ir_6$: C, 31.55; H, 3.96. Found: C, 31.96; H, 3.83. **8**: ^{1}H NMR (CD_3CN): δ 2.26 (s, 45H, Cp*). FAB MS (*m*-nitrobenzyl alcohol): 1133 ([**8**–BF_4]$^+$), 1046 ([**8**–$(BF_4)_2$]$^+$), 523 ([**8**–$(BF_4)_2$]$^{2+}$), all ions showed consistent isotopic patterns. **9**: ^{1}H NMR (CD_3CN): δ 2.39 (s, 60H, Cp*). FAB MS (*m*-nitrobenzyl alcohol): 1803 ([**9**–BF_4]$^+$) 1716 ([**9**–$(BF_4)_2$]$^+$), 1629 ([**9**–$(BF_4)_3$]$^+$), 814.5 ([**9**–$(BF_4)_3$]$^{2+}$), all ions showed consistent isotopic patterns. Anal. Calcd for $C_{40}H_{60}B_3F_{12}S_4Ir_4$: C, 25.41; H, 3.20. Found: C, 25.37; H, 3.20.

Preparation of 7. A mixture of **2**·0.5(Et_2O) (387 mg, 0.339 mmol) and KOBu^t (93 mg, 0.83 mmol) in THF (30 mL) was stirred at room temperature for 10 h. The resulting dark brown solution was evaporated to dryness, and the residue was successively extracted with hexane (total 70 mL). Evaporation of the solvent under vacuum afforded **7** as a dark brown solid (311 mg, 90% yield). ^{1}H NMR (C_6D_6): δ −20.98 (s, 2H, hydride), 2.16 (s, 45H, Cp*). Anal. Calcd for $C_{30}H_{47}SIr_3$: C, 35.45; H, 4.66. Found: C, 35.20; H, 4.65.

Reaction of 7 with HBF_4. To a benzene solution (5 mL) of **7** (52 mg, 0.051 mmol) was added $[Et_2OH][BF_4]$ (8.0 μL, 0.058

(52) Heinekey, D. M.; Fine, D. A.; Harper, T. G. P.; Michel, S. T. *Can. J. Chem.* **1995**, *73*, 1116.

(53) (a) Henderson, R. A. *Coord. Chem. Rev.* **2005**, *249*, 1841. (b) Henderson, R. A. *Chem. Rev.* **2005**, *105*, 2365.

(54) Budzelaar, P. H. M. *gNMR 4.1.0*; Charwell Scientific:The Magdalen Centre, Oxford Science Park, Oxford OX4 4GA, U.K.,1995−1999.

mmol) at room temperature. The dark brown solution gradually turned red on stirring, and a brown oil deposited. After 2.5 h, the resulting mixture was dried, and the residue was successively washed with Et_2O. Crystallization of the remaining solid from MeCN/Et_2O afforded reddish-orange plates of **2**·0.5(Et_2O) (41 mg, 71% yield).

Preparation of [(Cp*Ir)$_4$(μ_3-S)$_2$(μ-H)$_2$][BF$_4$]$_2$ (10). To a solution of **3** (74 mg, 0.051 mmol) in CH_2Cl_2 (5 mL) was added [Et_2OH][BF_4] (8.5 μL, 0.062 mmol) at room temperature with stirring. After the evolution of gas ceased, the resultant solution was stirred for 2 h. The solvent was evaporated in vacuo, and the residue was washed with THF (6 mL). Recrystallization from CH_2Cl_2 (3 mL)/hexane (15 mL) gave black plates of [(Cp*Ir)$_4$(μ_3-S)$_2$(μ-H)$_2$][BF_4]$_2$·0.5(CH_2Cl_2) (**10**·0.5(CH_2Cl_2), 75 mg, 93% yield). ^{1}H NMR (CD_3CN): δ −19.63 (s, 2H, hydride), 1.95, 2.19 (s, 30H each, Cp*), 5.44 (s, 1H, CH_2Cl_2). FAB MS (*m*-nitrobenzyl alcohol): 1463 ([**10**–BF_4]$^+$ with correct isotopic pattern). Anal. Calcd for $C_{40.5}H_{63}B_2F_8S_2ClIr_4$: C, 30.56; H, 3.99. Found: C, 30.49; H, 3.98.

Reaction of 10 with H$_2$ in the Presence of Pyridine. An MeCN (2 mL) solution containing **10**·0.5(CH_2Cl_2) (12 mg, 7.7 μmol) and pyridine (62 μL, 0.77 mmol) was stirred under 1 atm of H_2 atmosphere at 50 °C for 16 h. Determination by ^{1}H NMR spectroscopy using Ph_3CH as an internal standard revealed that yields of formed **3** and remaining **10** were 95% and 2%, respectively.

Reaction of 10 with H$_2$ in the Presence of Bu^{n}NH$_2$. To a solution of **10**·0.5(CH_2Cl_2) (80 mg, 0.051 mmol) in MeCN (15 mL) was added Bu^nNH_2 (50 μL, 0.51 mmol), and the mixture was stirred under 1 atm of H_2 at room temperature for 50 h. After evaporation of the volatiles, the resulting solid was washed with benzene (7 mL) and recrystallized from MeCN (1 mL)/ether (18 mL) to form black prisms (54 mg, 74% yield) containing **11** and **3** in a 7:1 ratio. In a different run, NMR yields of **11** and **3** in the reaction mixture were determined to be 82% and 13%, respectively. Cluster **11** formed an equilibrium mixture of two species, **11a** and **11b**, in solution, and the ratios of **11a**/**11b** were 91:9 in CD_3CN and 94:6 in $CDCl_3$. ^{1}H NMR (CD_3CN): **11a**: δ −15.69 (s, 1H, hydride), −12.99 (s, 2H, hydride), 1.71, 1.93 (s, 30H each, Cp*); **11b**: δ −16.80, −11.65 (d, J = 3.2 Hz, 1H each, hydride), −12.67 (s, 1H, hydride), 1.69, 1.80 (s, 15H each, Cp*), 2.00 (s, 30H, Cp*). Anal. Calcd for $C_{40}H_{63}BF_4S_2Ir_4$: C, 32.82; H, 4.34. Found for 7:1 mixture of **11** and **3**: C, 32.77; H, 4.21.

Reduction of 10 by Cp$_2$Co in the Presence of [Et$_3$NH][BF$_4$]. To a stirred MeCN (5 mL) solution containing **10**·0.5(CH_2Cl_2) (81 mg, 0.051 mmol) and [Et_3NH][BF_4] (11 mg, 0.056 mmol) was added Cp_2Co (20 mg, 0.11 mmol), and the mixture was stirred at room temperature for 2 h. Products were determined by ^{1}H NMR spectroscopy using Ph_3CH as an internal standard. Yields of **3**, **11**, and recovered **10** were 81%, 3%, and 2%, respectively, and quantitative conversion of Cp_2Co into Cp_2Co^+ (δ 5.66 in CD_3CN) was also confirmed.

Reduction of 10 by Cp*$_2$Co without Additives. To a solution of **10**·0.5(CH_2Cl_2) (80 mg, 0.050 mmol) in MeCN (5 mL) was added Cp^*_2Co (34 mg, 0.10 mmol) at −40 °C, and the mixture was gradually warmed to room temperature over 6 h with stirring. The resulting reddish-brown solution containing black precipitate was evaporated to dryness and extracted with toluene (5 mL). The residual brown solid majorly consisted of [Cp*Co][BF_4] (δ 1.69 in CD_3CN) and also contained a complicated mixture of iridium clusters. Addition of MeCN to the dark bluish-green toluene solution afforded dark blue crystals of [(Cp*Ir)$_3$(μ_3-S)$_2$] (**12**) after storage at −20 °C (19 mg, 36% yield vs Cl). ^{1}H NMR (C_6D_6): δ 1.90 (br, 30H, Cp*), 2.31 (br, 15H, Cp*). Anal. Calcd for $C_{30}H_{45}S_2Ir_3$: C, 34.43; H, 4.33. Found: C, 34.63; H, 4.26.

Preparation of [(Cp*Ir)$_4$(μ_3-S)$_2$(μ-H)$_2$(CO)][BF$_4$]$_2$ (13). A solution of **10**·0.5(CH_2Cl_2) (77 mg, 0.048 mmol) in MeCN (5 mL) was stirred at room temperature under CO atmosphere (1 atm) for 18 h. The resulting solution was concentrated to 3 mL, and ether (15 mL) was added. Black crystals of [(Cp*Ir)$_4$(μ_3-S)$_2$(μ-H)$_2$(CO)][BF_4]$_2$ (**13**) were filtered, washed with ether, and dried under a stream of N_2 (45 mg, 59% yield). ^{1}H NMR (CD_3CN): δ −16.75, −10.95 (d, J = 4.4 Hz, 1H each, hydride), 2.03, 2.09 (s, 15H each, Cp*), 2.06 (s, 30H, Cp*). IR (KBr): ν(C≡O) 1992 cm^{-1}. Anal. Calcd for $C_{41}H_{62}OB_2F_8S_2Ir_4$: C, 31.22; H, 3.96. Found: C, 30.92; H, 3.61.

Reaction of 10 with XyNC. To an MeCN solution (5 mL) of **10**·0.5(CH_2Cl_2) (81 mg, 0.051 mmol) was added XyNC (8 mg, 0.06 mmol) at 0 °C. After stirring the solution at 0 °C for 1 h, the crude products were determined by NMR measurement, which showed presence of *endo*-[(Cp*Ir)$_4$(μ_3-S)$_2$(μ-H)$_2$(CNXy)][BF_4]$_2$ (**14**), *exo*-[(Cp*Ir)$_4$(μ_3-S)$_2$(μ-H)$_2$(CNXy)][BF_4]$_2$ (**15**), **10**, and **8** in a 66:27:6:1 ratio. The resulting dark red solution was concentrated to 3 mL, and after addition of ether (18 mL) it was kept at −20 °C. Dark red crystals deposited were filtered off, throughly washed with ether, and dried under vacuum. Dark red prisms of **14** (47 mg, 63% yield) and red platelets of **15** (3 mg, 4% yield) were separated manually, and the remaining microcrystals (17 mg) contained **14** and **15** in a 1:1.8 ratio. **14**: ^{1}H NMR (CD_3CN): δ −16.88, −10.80 (d, J = 3.8 Hz, 1H each, hydride), 1.90, 2.07 (s, 15H each, Cp*), 2.03 (s, 30H, Cp*), 2.51 (s, 6H, Me of Xy), 7.2−7.4 (m, 3H, C_6H_3). IR (KBr): ν(C≡N) 2089 cm^{-1}. Anal. Calcd for $C_{49}H_{71}NB_2F_8S_2Ir_4$: C, 35.02; H, 4.26; N, 0.83. Found: C, 34.58; H, 4.25; N, 0.72. **15**: ^{1}H NMR (CD_3CN): δ −16.93, −12.54 (d, J = 3.2 Hz, 1H each, hydride), 1.63, 1.93 (s, 15H each, Cp*), 2.05 (s, 30H, Cp*), 2.50 (s, 6H, Me of Xy), 7.2−7.4 (m, 3H, C_6H_3). IR (KBr): ν(C≡N) 2118 cm^{-1}. Anal. Calcd for $C_{49}H_{71}NB_2F_8S_2Ir_4$: C, 35.02; H, 4.26; N, 0.83. Found: C, 35.12; H, 4.33; N, 0.74.

Preparation of [(Cp*Ir)$_4$(μ_3-S)$_2$(μ_2-H)$_2$(N_2H_4)$_2$][BF$_4$]$_2$ (16). Anhydrous hydrazine (56 μL, 1.8 mmol) was added to an MeCN solution (15 mL) of **10**·0.5(CH_2Cl_2) (460 mg, 0.289 mmol), and the mixture was stirred at room temperature for 96 h. After concentration of the resulting red solution to 10 mL, addition of ether (50 mL) formed red crystals of [(Cp*Ir)$_4$(μ_3-S)$_2$(μ_2-H)$_2$(N_2H_4)$_2$][BF_4]$_2$ (**16**, 270 mg, 58% yield). ^{1}H NMR (CD_3CN): δ −18.04 (s, 2H, hydride), 1.66, 2.25 (s, 15H each, Cp*), 1.85 (s, 30H, Cp*), 3.80 (br dd, 4H, J = 5.4, 4.2 Hz, terminal NH_2), 5.63 (br dt, 2H, J = 9.5, 4.2 Hz, coordinated NH_2), 6.29 (br dt, 2H, J = 9.5, 5.4 Hz, coordinated NH_2). IR (KBr): ν(N−H) 3268, 3301, 3363, 3388 cm^{-1}. Anal. Calcd for $C_{40}H_{70}N_4B_2F_8S_2Ir_4$: C, 29.77; H, 4.37; N, 3.47. Found: C, 29.62; H, 4.14; N, 3.16.

Crystallography. Single crystals of **3**, **4**, **5**, **6**·0.5(toluene), **11**, **13**, **14**·2(MeCN), **15**, and **16** were obtained by the procedures stated above except for those of **14**·2(MeCN), which were used immediately as picked up from the mother liqour. Recrystallization of **2** from CH_2Cl_2/hexane and **10** from acetone/hexane provided single crystals of **2**·0.5(CH_2Cl_2) and **10**·acetone, respectively, which were suitable for X-ray analysis.[55] Those were sealed in glass capillaries under argon and measured at ambient temperature by using a graphite-monochromatized Mo Kα source. Data collections of **2**·0.5(CH_2Cl_2), **3**–**5**, **10**·acetone, **13**, **15**, and **16** were done on a Rigaku AFC7R diffractometer by $\omega-2\theta$ scan techniques except for **13** (ω-scan), and the data were corrected for absorption (based on ψ-scans) and secondary extinction.[56] Diffraction data of **6**·0.5(toluene), **11**, and **14**·2(MeCN) were measured on a Rigaku Mercury CCD diffractometer, processed using the CrystalClear program package[57] and corrected for absorption by empirical methods. Corrections for Lorentz and polarization effects were also applied to all data. For **10**·acetone, a decay was observed during

(55) **2**·0.5(CH_2Cl_2): Anal. Calcd for $C_{30.5}H_{49}BF_4SClIr_3$: C, 31.95; H, 4. Found: C, 32.24; H, 4.26. **10**·acetone: Anal. Calcd for $C_{43}H_{68}OB_2F_8S_2Ir_4$: C, 32.13; H, 4.26. Found: C, 32.00; H, 4.22.

(56) Larson, A. C. In *Crystallographic Computing*; Ahmed, F. R., Ed.; Munksgaard: Copenhagen, 1970; pp 291–294..

(57) *CrystalClear 1.3.5*; Rigaku Corporation, 1998–2003.

Table 2. Crystallographic Data for 2·0.5(CH_2Cl_2), 3, 4, 5, 6·0.5(toluene), and 10·acetone

	2·0.5(CH_2Cl_2)	**3**	**4**	**5**	**6**·0.5(toluene)	**10**·acetone
formula	$C_{30.5}H_{49}BF_4SClIr_3$	$C_{40}H_{63}BF_4S_2Ir_4$	$C_{30}H_{49}SIr_3$	$C_{40}H_{66}SIr_4$	$C_{53.5}H_{80}S_5Ir_6$	$C_{43}H_{68}B_2OF_8S_2Ir_4$
fw	1146.70	1463.74	1018.44	1347.90	2036.84	1607.62
space group	$P2_1/c$ (no. 14)	$C2/c$ (no. 15)	$P\bar{1}$ (no. 2)	$P\bar{1}$ (no. 2)	$P\bar{1}$ (no. 2)	$P\bar{1}$ (no. 2)
a, Å	11.173(2)	17.805(3)	11.029(3)	11.453(3)	11.301(2)	10.884(2)
b, Å	14.410(3)	15.405(3)	11.169(2)	11.645(2)	14.447(2)	12.317(2)
c, Å	22.428(1)	16.135(6)	15.158(2)	18.203(3)	19.471(4)	20.448(2)
α, deg	90	90	71.73(1)	76.79(1)	86.747(6)	91.34(1)
β, deg	103.447(7)	96.77(2)	73.04(2)	72.28(1)	84.344(6)	96.44(1)
γ, deg	90	90	63.92(2)	66.01(2)	68.362(5)	113.96(1)
V, Å^3	3512(1)	4394(1)	1566.5(5)	2097.4(7)	2939.7(9)	2481.9(6)
Z	4	4	2	2	2	2
ρ_{calcd}, g cm^{-3}	2.169	2.212	2.159	2.134	2.301	2.151
μ, mm^{-1}	11.547	12.246	12.830	12.759	13.775	10.865
cryst size, mm^3	0.25 × 0.12 × 0.02	0.15 × 0.12 × 0.03	0.3 × 0.3 × 0.12	0.4 × 0.35 × 0.3	0.3 × 0.1 × 0.05	0.35 × 0.35 × 0.2
transmn factor	0.338–1.000	0.378–1.000	0.227–1.000	0.685–1.000	0.538–1.000	0.296–1.000
no. of reflns unique (R_{int})	8060 (0.028)	5041 (0.032)	9144 (0.032)	9606 (0.032)	13 363 (0.034)	11 380 (0.087)
no. of reflns obsd ($F_o^2 > 2\sigma(F_o^2)$)	5175	3145	7575	8172	8881	7322
no. of variables	439	262	369	442	630	612
R_1[a]	0.042	0.044	0.050	0.045	0.051	0.049
final value of minimized R_w[b] or wR_2[c]	0.052[b]	0.053[b]	0.055[b]	0.056[b]	0.149[c]	0.057[b]
gof[d]	1.012	1.013	1.028	1.057	1.001	1.030

[a] $R_1 = \sum||F_o| - |F_c||/\sum|F_o|$ for $F_o^2 > 2\sigma(F_o^2)$. [b] $R_w = [\sum w(|F_o| - |F_c|)^2/\sum w(F_o)^2]^{1/2}$ ($w = [\sigma(F_o^2) + aF_o^2 + b]^{-1}$) for observed data. [c] $wR_2 = [\sum w(F_o^2 - F_c^2)^2/\sum w(F_o^2)^2]^{1/2}$ ($w = [\sigma(F_o^2) + aF_o^2 + b]^{-1}$) for all unique data. [d] gof = $[\sum w(|F_o| - |F_c|)^2/\{$(no. of reflns obsd) − (no. of variables)$\}]^{1/2}$ or $[\sum w(F_o^2 - F_c^2)^2/\{$(no. of reflns obsd) − (no. of variables)$\}]^{1/2}$, when minimized parameter is R_w or wR_2, respectively.

Table 3. Crystallographic Data for 11, 13, 14·2(MeCN), 15, and 16

	11	**13**	**14**·2(MeCN)	**15**	**16**
formula	$C_{40}H_{63}BF_4S_2Ir_4$	$C_{41}H_{62}B_2OF_8S_2Ir_4$	$C_{53}H_{77}B_2N_3F_8S_2Ir_4$	$C_{49}H_{71}B_2NF_8S_2Ir_4$	$C_{40}H_{70}B_2N_4F_8S_2Ir_4$
fw	1463.74	1577.55	1762.82	1680.71	1613.63
space group	$C2/c$ (no. 15)	$P2_1/c$ (no.14)	$P\bar{1}$ (no. 2)	$P2_12_12_1$ (no. 19)	$P2_1/n$ (no.14)
a, Å	16.568(5)	17.108(3)	13.265(5)	13.632(4)	13.004(1)
b, Å	16.443(5)	23.391(3)	15.434(6)	18.821(8)	17.453(4)
c, Å	16.309(5)	23.447(4)	15.850(7)	20.586(4)	21.917(2)
α, deg	90	90	82.61(1)	90	90
β, deg	91.138(4)	90.83(1)	73.72(1)	90	97.836(7)
γ, deg	90	90	70.58(1)	90	90
V, Å^3	4442(2)	9381(2)	2935(2)	5281(3)	4927(1)
Z	4	8	2	4	4
ρ_{calcd}, g cm^{-3}	2.189	2.234	1.994	2.114	2.175
μ, mm^{-1}	12.116	11.495	9.197	10.216	10.945
cryst size, mm^3	0.15 × 0.1 × 0.05	0.4 × 0.4 × 0.3	0.35 × 0.3 × 0.25	0.4 × 0.25 × 0.2	0.3 × 0.3 × 0.2
transmn factor	0.550–1.000	0.328–1.000	0.510–1.000	0.499–1.000	0.691–1.000
no. of reflns unique (R_{int})	5309 (0.044)	16 489 (0.033)	12 666 (0.044)	7507 (0.043)	11 265 (0.103)
no. of reflns obsd ($F_o^2 > 2\sigma(F_o^2)$)	2796	11 520	9909	7348	6082
no. of variables	297	1116	737	690	583
R_1[a]	0.041	0.043	0.053	0.037	0.065
Final value of minimized R_w[b] or wR_2[c]	0.134[c]	0.054[b]	0.136[c]	0.047[b]	0.071[b]
gof[d]	1.012	1.017	1.004	1.001	1.011

[a] $R_1 = \sum||F_o| - |F_c||/\sum|F_o|$ for $F_o^2 > 2\sigma(F_o^2)$. [b] $R_w = [\sum w(|F_o| - |F_c|)^2/\sum w(F_o)^2]^{1/2}$ ($w = [\sigma(F_o^2) + aF_o^2 + b]^{-1}$) for observed data. [c] $wR_2 = [\sum w(F_o^2 - F_c^2)^2/\sum w(F_o^2)^2]^{1/2}$ ($w = [\sigma(F_o^2) + aF_o^2 + b]^{-1}$) for all unique data. [d] gof = $[\sum w(||F_o| - ||F_c||)^2/\{$(no. of reflns obsd) − (no. of variables)$\}]^{1/2}$ or $[\sum w(F_o^2 - F_c^2)^2/\{$(no. of reflns obsd) − (no. of variables)$\}]^{1/2}$, when minimized parameter is R_w or wR_2, respectively.

the data collection (−13%), and a correction was done. Details of the X-ray diffraction study are listed in Tables 2 and 3.

Structure solution and refinements were carried out by using the CrystalStructure program package.[58] The positions of the non-hydrogen atoms were determined by Patterson methods (PATTY)[59] and subsequent Fourier synthesis (DIRDIF 99).[60] They were refined by full-matrix least-squares techniques with anisotropic thermal parameters except for some atoms in the disordered fragments, which were refined isotropically (Cp* ligands in **5**, **6**·0.5(toluene), **10**·acetone, **13**, and **16**; BF_4 anions in **10**·acetone, **15**, and **16**; toluene molecule in **6**·0.5(toluene)). The hydrido ligands in **2**·0.5(CH_2Cl_2) and **4** were found in difference Fourier maps and refined with isotropic parameters. The C-H hydrogen atoms except for those attached to the disordered fragments were placed at the calculated positions and included in the final stages of the refinements with fixed parameters. Analysis of **11** showed the existence of some disorder in the cluster core, which is presumably caused by cocrystallization with **3**. One of two independent Ir atoms was split into two positions with 90.5% and 9.5% occupancies, representing **11** and **3**, respectively. The S atom was also distributed at two positions, probably due to cocrystallization as well as the nearly D_{2d}-symmetrical $(Cp^*Ir)_4$ framework of

(58) *CrystalStructure 3.6.0*, Crystal structure analysis package; Rigaku and Rigaku/MSC: The Woodlands, TX, 2000–2004.

(59) PATTY: Beurskens, P. T.; Admiraal, G.; Beurskens, G.; Bosman, W. P.; Garcia-Granda, S.; Gould, R. O.; Smits, J. M. M.; Smykall, C. *The DIRDIF program system*; Technical Report of the Crystallography Laboratory; University of Nijmegen: The Netherlands, 1992.

(60) DIRDIF99:Beurskens, P. T.; Admiraal, G.; Beurskens, G.; Bosman, W. P.; de Gelder, R.; Israel, R.; Smits, J. M. M. *The DIRDIF-99 program system*; Technical Report of the Crystallography Laboratory; University of Nijmegen: The Netherlands, 1999.

11, and they were treated as 86.5% and 13.5% atomic probabilities. The absolute structure of **15** was determined by refinement of the Flack parameter ($x = 0.06(2)$).[61]

Acknowledgment. This work was supported by a Grant-in-Aid for Scientific Research on Priority Area (No. 18065005, "Chemistry of Concerto Catalysis") from the Ministry of Education, Culture, Sports, Science, and Technology, Japan, and by CREST of JST (Japan Science and Technology Agency).

Supporting Information Available: X-ray crystallographic files in CIF format are available free of charge via the Internet at http://pubs.acs.org.

(61) Flack, H. D. *Acta Crystallogr., Sect. A* **1983**, *A39*, 876.

OM701207J